A THESIS

ON

DEVELOPMENT OF ALUMINIUM BASED BEARING ALLOYS

Submitted in partial fulfillment of the requirements for the award of the degree of

Master of Technology (M.Tech.)

IN

MATERIALS SCIENCE AND ENGINEERING

Submitted By

KAMALPREET KAUR

Roll No. 6050503

Under the Guidance of

Dr. O. P. PANDEY

Professor, SPMS

T.U., Patiala, Punjab (147004)

SCHOOL OF PHYSICS AND MATERIAL SCIENCES
THAPAR UNIVERSITY
PATIALA (PUNJAB)-147004, INDIA.

JUNE 2007.

CERTIFICATE

This is to certify that the thesis entitled "**Development of Aluminium based Bearing Alloys"** submitted by **Miss Kamalpreet Kaur** in the partial fulfillment of the requirement for the award of the degree of **M. Tech** in **Materials Science and Engineering** from the **School of Physics and Materials Science, Thapar University, Patiala,** is a record of candidate's own work carried out by her under my supervision and guidance. The matter embodied in this report has not been submitted in part or full to any other university or institute for the award of any degree.

(Dr.O.P.PANDEY)

Professor, SPMS

Thapar University,

Patiala, Punjab (147004)

Countersigned by:

(Dr. O.P. Pandey)
Professor and Head, SPMS
Thapar University,
Patiala, Punjab (147004).

(Mr. R.K. Sharma)
Dean, Academic Affairs
Thapar University,
Patiala, Punjab (147004).

ACKNOWLEDGEMENT

I express my deep gratitude and respects to my guide **Dr. O.P. Pandey, Professor and Head, School of Physics and Materials Science** for his keen interest and valuable guidance, strong motivation and constant encouragement during the course of the work. I thank him from the bottom of my heart for introducing me to the science of fuel cells. I thank him for his great patience, constructive criticism and myriad useful suggestions apart from invaluable guidance to me.

I am grateful to **Dr. Kulvir Singh, Assistant Professor and PG Incharge, SPMS and Dr. Sanjeev Das, lecturer, SPMS** for their encouragement and execution of thesis work.

I would also like to thank **Dr. K. K. Raina, Professor and Deputy Director,** for his constant guidance and encouragement.

It gives me immense pleasure to express my special thanks to **Mr.P.K.Singh** and **Jant Singh** who always took keen interest in guiding me during my work. I wish my sincere thanks to **Ms Anu Arora, Mr. Vishal Kumar, Ms Shefali** and **Ms Zinky Jindal** for their cooperation.

I owe my sincere thanks to all the staff members of **School of Physics and Materials Science** for their support and encouragement. I would also like to thank my all marvelous friends for extending their whole hearted support.

Last but not the least; I would like to thank my parents and my brother for their moral support that kept my spirit up during the endeavor.

Kamalpreet Kaur

Dedicated To
My Parents

INDEX

CONTENTS **PAGE NUMBER**

ABSTRACT

In order to develop a good bearing alloy for structural applications in industries, the present work was planned. Before testing the mechanical properties including bearing property it is essential to understand their structural features as structure is going to govern the property. Considering this aspect the proposal was planned. The thesis describes about the different bearing alloys used in industry, their properties and limitations. In order to overcome these limitations, some idea was planned and accordingly experiments were designed and performed. Among the end application, one of the applications is piston alloys where distribution of silicon phase is considered to be important to achieve good mechanical strength alongwise good wearing property. Considering this fact alloys of near eutectic composition (hyperside) were made. In order to understand the distribution of silicon phase different alloying elements were added. These influence the development of varieties of structure. The present work emphasizes on the structural features of these alloys.

CHAPTER – 1

INTRODUCTION

1.1 Bearings

Bearings are devices used to transmit loads between relatively moving surfaces. These are basically used to ease friction between moving parts. They find application in rotating parts of virtually all machines and automobiles. The automobile industry is the major user segment for bearings, followed by general engineering, heavy industries and railways.

Bearings are produced in various sizes and shapes with the smallest bearing weighing just a few grams and the larger ones weighing a few tonnes. The material used to produce bearings can also vary from conventional steel to ceramics, brass and plastics. Bearings can be broadly classified into two segments:

(a) Anti-friction bearings

(b) Bimetals

1.1.1 Anti-friction bearings: Rolling contact bearings are often referred to antifriction bearings. Antifriction bearings, as their name implies, minimize friction by removing any possible sliding between bearing surfaces and replacing all contacts with rolling interfaces. The main components of an anti-friction bearing are the inner ring, the outer ring, the rolling elements, the cage and the seals as shown in figure 1.1. The anti-friction roller bearings can be further sub-classified based on the size of the rolling element. Depending on the type of the rolling elements that are used, the anti-friction bearings segment can be classified into ball bearings and roller bearings. The balls in a ball bearing transfer the load on a very small surface. The load carrying capacity is therefore lower than for a roller bearing, where rollers transfer the load via a larger line of contact with the raceways or the outer surface.

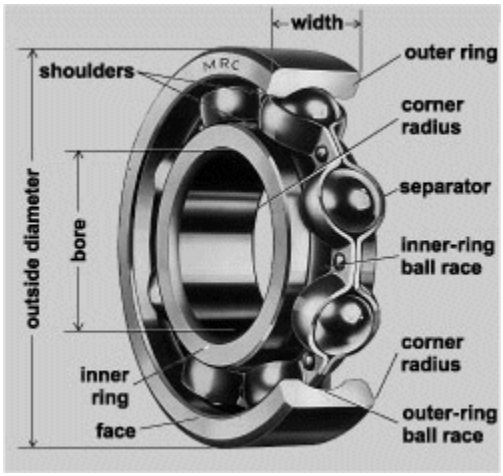

Figure 1.1: Schematic figure of anti friction ball bearing.

1.1.1.1 Faults in the roller bearings:

Rolling-element bearings often work well but sometimes minor problem cause bearing to fail quickly and mysteriously. For example with a stationary (non-rotating) load, small vibrations can gradually press out the lubricant between the rollers and races (false brinelling). Without lubricant the bearing fails, even though it is not rotating and thus is apparently not being used.

There are three usual limits to the lifetime or load capacity of bearings: abrasion, fatigue and pressure induced welding.

a) Abrasion: Abrasion is when the surface is eroded by hard contaminant scraping at the bearing materials.

b) Fatigue: Fatigue is when material breaks after it is repeatedly bent and released. Where the ball or roller touches the race is always some bending and hence a risk of fatigue. Smaller balls or rollers bend more sharply and so tend to fatigue faster.

c) Pressure induced welding: Pressure induced welding is when two metal pieces are pressed together at very high pressure and they become one. Although balls rollers and

races may look smooth, they are microscopically rough. Thus there are high pressure spots which push away the bearing lubricant. Sometimes, the resulting metal to metal contact welds a tiny part of the ball or roller to the race. As the bearing continue to rotate, the weld is then torn apart, but it may leave race welded to bearing or bearing welded to race.

Although there are many other apparent causes of bearing failure but broadly speaking it can be reduced to these three. For example, a bearing which is run dry of lubricant fails not because it is “without lubricant”, but because lack of lubricant leads to fatigue and welding, and the resulting wear debris can cause abrasion. Similar vents occur in false brinelling damage.

1.1.2 Bimetal bearings: Bimetal bearings (also known as engine bearings) are primarily used in the engines of automobiles or machines. A Bimetal bearing is a component made out of steel strip lined with bearing material (non-ferrous metal alloys). They are meant to reduce the friction between the moving parts such as in the crank shaft, connecting rod and cam shaft assemblies of any (prime mover) engine or equipment with reciprocating and revolving systems. It finds application in all varieties of diesel engines, petrol engines and air compressors. Bimetal bearings are of three types — bearing half, bush and washer. These can be seen in the figure1.2 given below:

Figure 1.2: Bimetal bearings of different sizes.

a) Plain bearing is a bearing which carries load by sliding. Plain bearing is often called a bushing or babbit. Plain bearings are widely used in most of automobiles. A typical plain bearing is made up of two parts. For example a rotary plain bearing can be just a shaft running through hole. A simple linear bearing can be a pair of flat surfaces designed to allow motion, for example a drawer and the slides it rests on.

Plain bearings are relatively simple and hence inexpensive. They are also compact, light weight, straightforward to repair and have high load carrying capacity. Plain bearings may carry the load in several ways depending on their operating conditions, load relative surface speed, quality and quantity of lubricant and temperature (affecting lubricant viscosity). If the bearings load is carried solely by a film of fluid lubricant, there being no contact between the two bearing surfaces. In these conditions they are known as fluid bearings. In mixed conditions, load is carried partly by direct surface contacts and partly by a film forming between the two. In dry conditions, the full load is carried by surface to surface contact.

Under dry conditions when fluid bearings operate may wear faster and have high friction than rolling element bearing at the startup and shutdown. Plain self-lubricant bearing utilize porous journals within which a lubricant is held. As the bearing operates and lubricant is displaced from the bearing surface, more is carried in from non wear parts of bearing. Babbit metal is characterized by its resistance to galling. Common compositions for Babbit alloys used in industries:

- 90% tin 10% copper
- 89% tin 7% antimony 4% copper
- 80% lead 15% antimony 5% tin

Babbit metal is soft and easily damaged, and seems at first sight an unlikely candidate for a bearing surface, but this appearance is deceptive. The structure of the alloy is made up of small hard crystals dispersed in a matrix of softer alloy. As the bearing wears the harder crystal is exposed, with the matrix eroding somewhat to provide a path for the lubricant between the high spots that provide the actual bearing surface.

1.2 Material properties:

For a good bearing properties the babbit alloys must possess following properties:-

- Load Carrying Capaity
- Wear Rate
- Fatigue resistance
- Good heat dissipation
- Corrosion resistance
- Embedability
- Comformability
- Temperature Strength
- Compatibility

However, soft materials are inherently weak and therefore have a limited load capacity (leading to extrusion) and fatigue resistance (leading to crack formation). In addition to the ability of soft materials to conform to the mating surface, other advantages are also important. The ability to embed dirt and other abrasive contamination helps to minimize damage to the surfaces. Also the inherent low shear strength of soft materials reduces the risk of seizure occurring due to high rubbing temperatures if contact occurs. The compromise solution for bearings is to use soft materials in combination with hard materials. Abrasive wear resistance can substantially be improved by second phases embedded in a hard or soft matrix [1].In this way there is a trade-off between the tribological properties (conformability, embeddability and resistance to seizure) and the mechanical properties (strength and fatigue resistance).Basically babbit materials are Sn, Al and Cu based for bearing material in which either material is soft or second phase is soft. Babbit materials are characterise into two categorories:

1. Substance with hard matrix and soft second phase
2. Substance with soft matrix and hard second phase

Among these categories, the babbit alloys which have been developed are:

- Tin based
- Aluminium based
- Copper based

Metal-matrix composites (MMCs) exhibit the ability to withstand high tensile and compressive stresses by the transfer and distribution of the applied load from the ductile matrix to the reinforcement phase. In situ composite structures, such as aluminium containing silicon in amounts above the solubility limit, are formed by solidification. However, the compositions and relative amounts of the two phases are limited to a narrow range, controlled by growth kinetics and equilibrium conditions.

1.3 Aluminium bearing materials

Aluminium alloys with desirable bearing properties are used in a wide variety of applications. Steel-backed and solid aluminium bearings are employed as connecting rod and main bearings in internal combustion engines and industrial compressors. Other aluminium bearing applications are in heavy tooling, such as boring mills, presses, lathes, milling machines, and grinding mills, and as hydraulic pump bushings. Aircraft landing gear assemblies, power shovels, and track rollers utilize solid aluminium bearings to withstand high-shock loads. Rolling mill bearings are cast of aluminium alloys to increase load and speed capability. Aluminium bushings are normally employed for relatively light, low-speed duty, compared to bearings, and they are made from aluminium bearing or other alloys, depending on the frictional and mechanical properties required for the application.

Aluminium alloys, such as the 2000, 5000, 6000 and 7000 alloy series, are the most commonly utilized materials in composite fabrication. Aluminium composites are widely employed in the aerospace industry. Al-Si based composites such as A356 (Al,7Si,0.3Mg) that contain $A1_20_3$, ZrO particles or SiC particles are used in the fabrication of automotive engine components. Wear resistance and operating properties of aluminium cast diesel pistons are enhanced by the use of aluminium-based composite piston ring inserts.

In this project, an attempt has been made to add Pb, Sn, Cd and Bi separately to aluminium-silicon alloys. Silicon also has a low density (2.34 g cm^{-3}), which may be an advantage in reducing the overall weight of the cast component. Silicon has a very low solubility in aluminium; it therefore precipitates as virtually pure silicon, which is hard and hence improves the abrasion resistance. However, silicon melting temperature is 1414^{o}C which is quite high. However, it decreases upto 577 ^{o}C at eutectic composition.

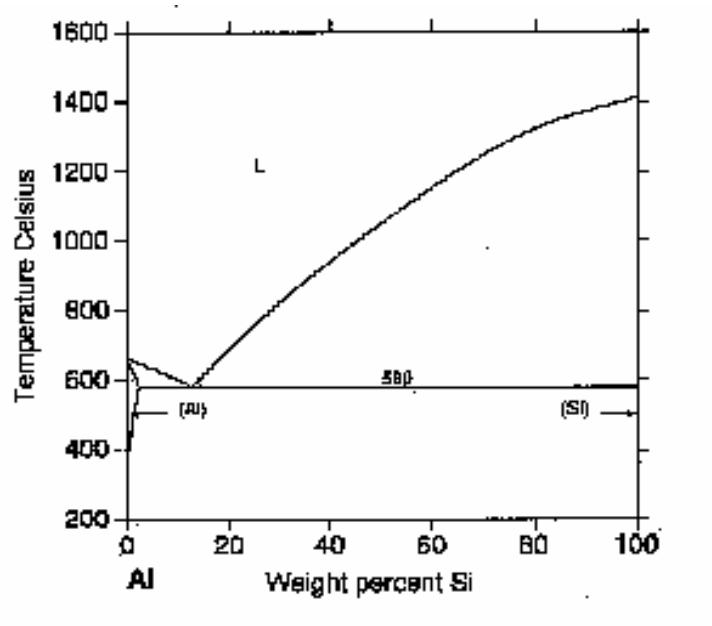

Figure1.3:Aluminium-silicon phase diagram.

Aluminium-silicon alloys form a eutectic at 12.6 wt% silicon, the eutectic temperature for this is 577 ^{o}C as shown in figure1.3. This represents a typical composition for a casting alloy because it has the lowest possible melting temperature. Al-12.6Si wt% alloys are therefore common.

Copper is the most important alloying element for aluminium. The 2xxx aluminium group contains copper which is added for strength achieved by precipitation hardening although the corrosion resistance tends to worsen. An aluminum-copper alloy comprising substantially insoluble particles which occupy the interdendritic regions of the alloy is shown in figure1.4. The copper melting point is 1083 ^{o}C which reduces to 548 ^{o}C at eutectic composition of 33wt% copper. Aluminium-copper alloys are most important

alloys which shows precipitation hardening phenonomenon i.e. after giving them a heat treatment at desired temperature, it will provide maximum hardness.

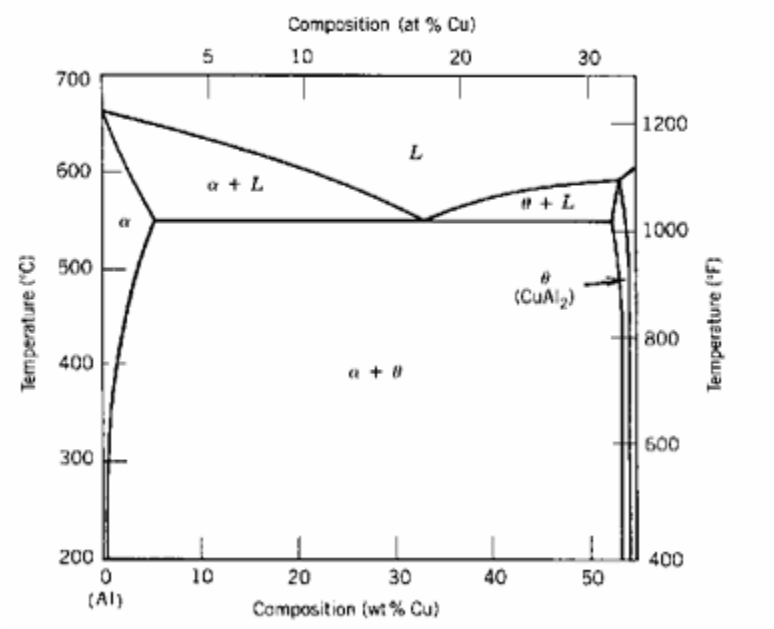

Figure1.4: Aluminium-copper phase diagram

The Al-Sn phase diagram (Figure 1.5) shows many of the features of an ideal solidifying system. Al and Sn exhibit mutual insolubility in the solid phase, form no intermetallic phases and the liquids are miscible.

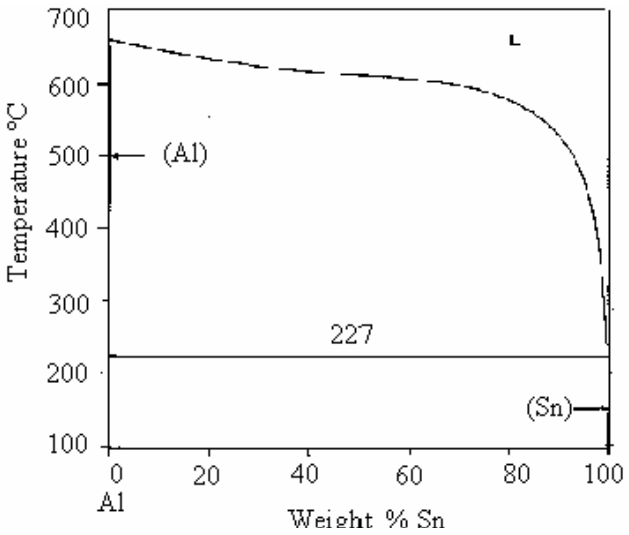

Figure 1.5: Al- Sn phase diagram

Additionally, the melting point of tin ($232^{O}C$) is much lower than that of aluminium ($660^{O}C$). A higher Sn alloy could be utilized as a bearing material, in which case the increased Sn content may be beneficial in both the elimination of porosity and as a solid lubricant.

A similar result has been found with Pb additions and is due to the lubricity of the Pb. Addition of lead in small quantities improves the machinability of the aluminium alloy. Also Lead containing bearings have the advantage of good lubrication. However, their chief advantage is their low cost. Al-Pb phase diagram is shown in Figure 1.6 for reference.

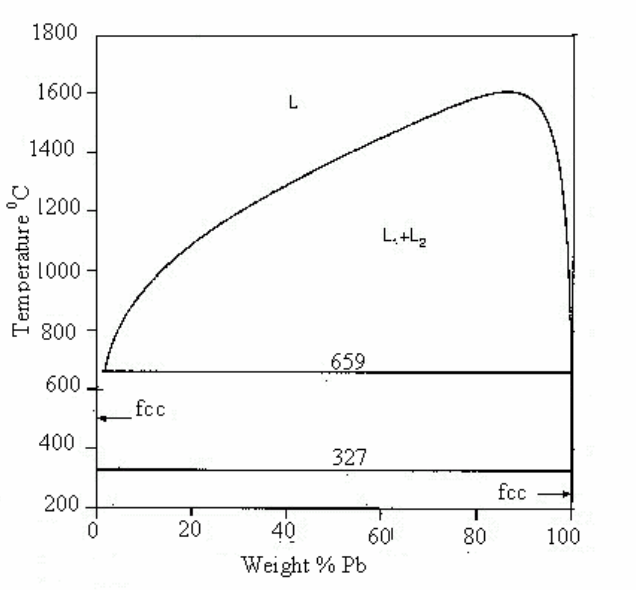

Figure 1.6: Al-Pb Phase diagram

1.4 Objective

The increasing demand from many industries for improved properties in materials has stimulated the development of new materials. For the automotive industry, the properties most required are reduced weight, low thermal expansion coefficient and excellent mechanical properties; mainly wear resistance at high temperatures. In this context, various new materials such as the Al-Si alloys have been considered. Of particular

interest are the Al-Si-Cu alloys with hypereutectic compositions, due to their optimum wear resistance. This is a consequence of the large volumetric fraction of primary silicon phase in the alloy. The optimum mechanical properties due to a fine and homogeneous distribution of the primary silicon phase in the aluminium matrix. These are light materials with high wear resistance, and this particular property is important for some motor parts, such as cylinder liners. In fact, spray formed Al-Si-Cu alloys have been recently used for the manufacture of cylinder liners where wear resistance is essential. Further, these alloys are light, have low thermal expansion coefficient, oxidation resistance at high temperatures and high hardness. During solidification of Al-Si-Cu alloys, Si needles which form eutectic is distributed as fine and coarse particle. The immisible elements like Sn, Pb influence the structure by either attracting them or by repelling them. In order to study their influence on structural features these elements have been knowingly added in small quantity. The present report describes their structural features in detail.

CHAPTER – 2

AGE HARDENING OF ALUMINIUM ALLOYS

2.1 Introduction

Precipitation hardening, also called **age hardening** or **dispersion hardening**, is a heat treatment technique used to strengthen malleable materials, especially non-ferrous alloys including most structural alloys of aluminium and titanium. It relies on changes in solid solubility with temperature to produce fine particles of an impurity phase, which impede the movement of dislocations, or defects in a crystal's lattice. Since dislocations are often the dominant carriers of plasticity (deformations of a material under stress), this serves to harden the material. The impurities, in fact, play the same role as matrix substances in composite materials. Just as the formation of ice in air can produce clouds, snow, or hail, depending upon the thermal history of a given portion of the atmosphere, precipitation in solids can produce many different sizes of particles, which have radically different properties. Unlike ordinary tempering, alloys must be kept at elevated temperature for hours to allow precipitation to take place. This time delay is called **aging**.

Precipitation or age hardening was discovered by Alfred Wilm in Germany in 1906. He attempted to harden an alloy of essentially aluminum-2 atom percent copper in an analogous way to steels by a quenching treatment. The specimen was initially soft, but the hardness increased with time at room temperature after the quench

This process provides one of the most widely used mechanisms for the strengthening of metal alloys. In an attempt to understand the dramatic strengthening of this alloy, Paul D. Merica and his coworkers [2] studied both the effect of various heat treatments on the hardness of the alloy and the influence of chemical composition on the hardness. Among the most significant of their findings was the observation that the solubility of $CuAl_2$ in aluminum increased with increasing temperature. Although the specific phases responsible for the hardening turned out to be too small to be observed directly, optical

examination of the microstructures provided an identification of several of the other phases that were present.

In his Institute of Metals lecture [1], Merica summarized the Merica, Waltenberg, and Scott paper as follows: The four principal features of the original Duralumin theory were these:

(1) age-hardening is possible because of the solubility-temperature relation of the hardening constituent in aluminum,
(2) the hardening constituent is $CuAl_2$,
(3) hardening is caused by precipitation of the constituent in some form other than that of atomic dispersion, and probably in fine molecular, colloidal or crystalline form, and
(4) the hardening effect of $CuAl_2$ in aluminum was deemed to be related to its particle size.

2.2 Kinetics versus thermodynamics

This technique exploits the phenomenon of supersaturation, and involves careful balancing of the driving force for precipitation and the thermal activation energy available for both desirable and undesirable processes.

Nucleation occurs at a relatively high temperature (often just below the solubility limit) so that the kinetic barrier of surface energy can be more easily overcome and the maximum number of precipitate particles can form. These particles are then allowed to grow at lower temperature in a process called *aging*. This is carried out under conditions of low solubility so that thermodynamics drive a greater total volume of precipitate formation.

Diffusion's exponential dependence upon temperature makes precipitation strengthening, like all heat treatments, a fairly delicate process. Too little diffusion (*under aging*), and the particles will be too small to impede dislocations effectively; too much (*over aging*), and they will be too few and far between to interact with the majority of dislocations.

Age hardening behaviour of discontinuously reinforced aluminium matrix composites has been a subject of great interest both from scientific and technological view points. The nature of change in kinetics and magnitude of hardening during aging of these composites depend on

(a) matrix material [3,4],
(b) type of reinforcement including its size, shape and volume fraction [4-6],
(c) method of processing the composite [4],
(d) post fabrication treatment [7,8] and
(e) temperature of aging [3,4].

2.3 Aging Process

Aluminum, as well as some alloys, such as high-nickel steels, is subject to a two-stage phenomenon known as solution heat treatment and aging.

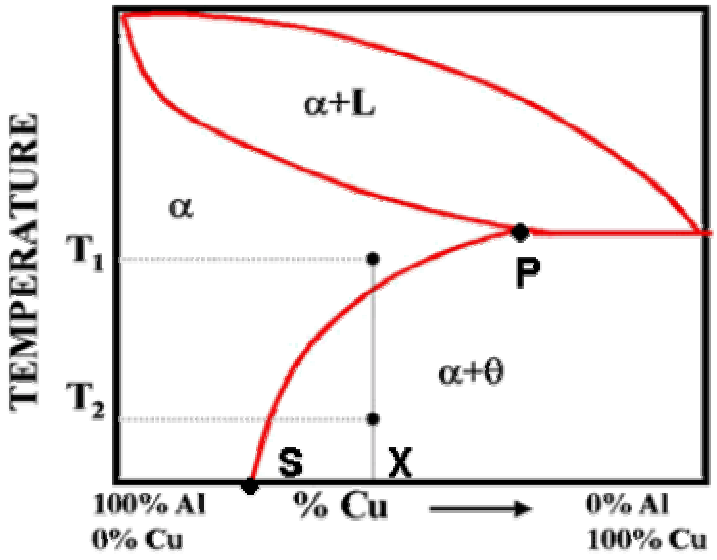

Figure 2.1: Age -hardening heat treatment phase diagram

2.3.1 Solution Heat Treating

Considering the age-hardening process of aluminum-copper alloys, the process involves a solution heat treatment at about 265 ^{o}C in which

1. the $CuAl_2$ phase is dissolved in the matrix,
2. the alloy is quenched to room temperature to retain the solid solution formed at high temperature,
3. following the quench, the alloy is either aged naturally (i.e., held at room temperature) or aged artificially by heating at a relatively low temperature (93 to 204 ^{o}C).

Figure 2.1 shows the solubility line PS, which indicates a decrease in solubility of the θ phase in the α phase as the temperature decreases. If a metal with composition X is heated above the solubility line to a temperature T_1, the phase θ will dissolve and uniformly disperse into the homogeneous solid α solution. Upon slow cooling, the phase will reform, and below PS solubility line the metal will once again consist of two distinct phases, θ and α.

If the metal with composition X is heated to T_1, and quenched, the dispersed submicroscopic phase is trapped in the α solution. The solution α is said to be supersaturated, because it contains more θ particles at room temperature than it can hold in its lattice structure. This process is called solution heat-treating. Figures 2.2 and 2.3 show the changes in microstructure as a result of quenching.

2.3.2 Aging

The supersaturated solid solution is unstable and if, left alone, the excess θ will precipitate out of the α phase. This process is called aging. There are three types of aging:

- Natural aging
- Artificial aging
- Abnormal aging

2.3.2.1 Natural Aging

When the process occurs at room temperature, it is called natural aging.

2.3.2.2 Artificial Aging

If the material that has been solution heat treated requires a heating to speed up the precipitation, the process is called artificial aging. It should be noted that freezing the solution heat treated material will retard the aging process.

2.3.2.3 Abnormal Aging

In many instances aging will occur without precipitation. The particle may actually diffuse within the lattices and distort them. This type of aging is called abnormal aging.

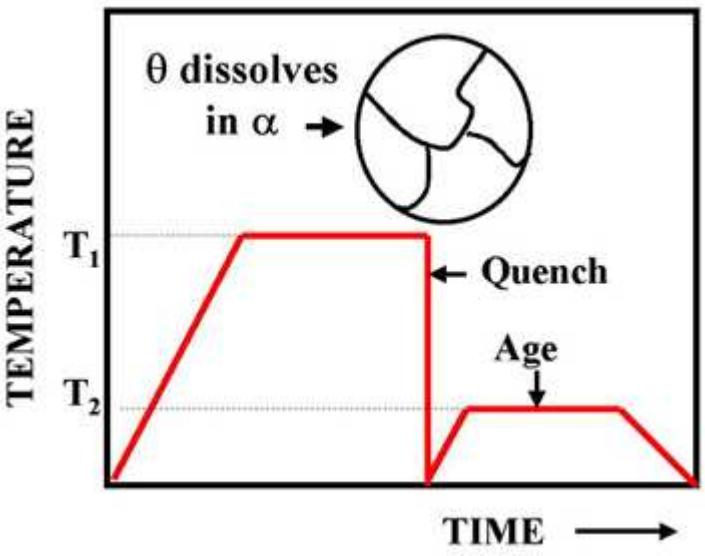

Figure 2.2: Aging process graph between temperature vs time.

After solution heat treatment the material is ductile, since no precipitation has occurred. Therefore, it may be worked easily. After a time the solute material precipitates and hardening develops. As the composition reaches its saturated normal state, the material reaches its maximum hardness.

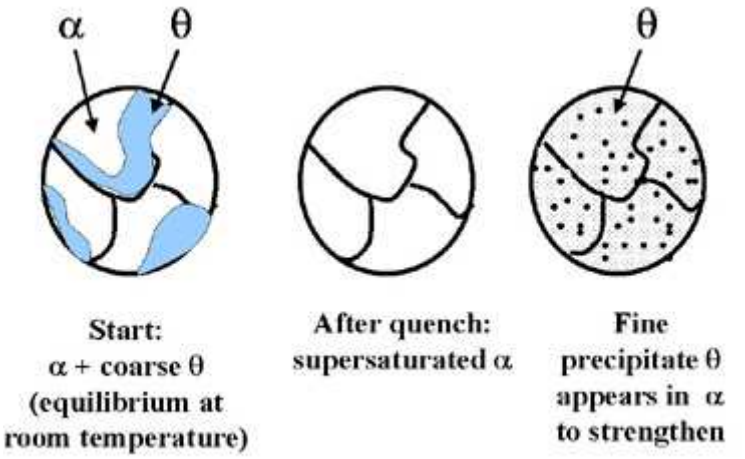

Figure 2.3: Microstructural features on precipitation hardening.

The precipitate, however, continues to grow. The fine precipitates disappear. They have grown larger, and as a result the tensile strength of the material decreases. This is called overaging. The hardness and tensile strength variation during aging and overaging are shown in Figure 2.4.

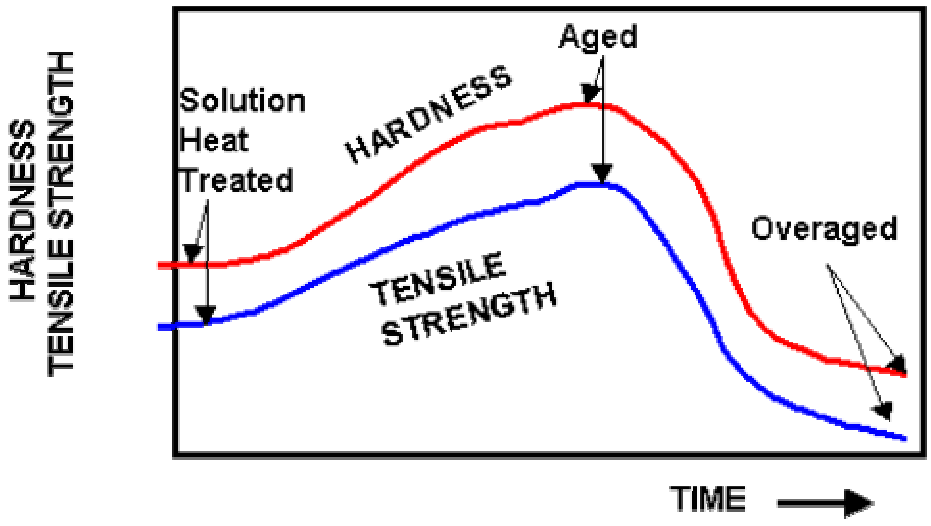

Figure 2.4: Hardness and Tensile Strength and Aging stages.

Table 2.1: Effect of aging on the properties of Aluminum Alloy 2014.

ALLOY AND CONDITION	TENSILE STRENGTH (Pa)	YIELD STRENGTH (Pa)	ELONGATION % IN 2 IN.	HARDNESS BHN 500 KG 10 MM
Annealed	1.86×10^8	9.65×10^7	18	45
Solution treated. Naturally aged	4.27×10^8	2.90×10^8	20	105
Solution treated, artificially aged	4.83×10^8	4.14×10^8	13	135

As mentioned earlier, refrigeration retards the aging process. At 0^oC (32^oF) the beginning of the aging process is delayed for several hours and freezing at temperatures of up to -73.3^oC ($-100\ ^oF$) retards aging for an extended period. Use is made of this fact in the aircraft industry when aluminum-alloy rivets, which normally age at room temperature, are kept in deep-freeze refrigerators until they are driven. The rivets have previously solution-treated, and as a single phase they are very ductile. After being driven, aging takes place at room temperature, with a resulting increase in strength and hardness.

However, with the treatment to give maximum hardness, in general precipitate particles are not visible with the highest-resolution light microscope. When the particles are visible the alloy has overaged. Not only is the hardness less in the overaged state but usually the alloy is very much less ductile compared to maximum hardness.

The mystery was solved first in aluminum-copper alloys independently by Guinier and Preston in 1937 by careful X-ray diffraction work. Diffuse scattering occurs outside but associated with the Bragg reflections of the solid solution, and these are due to regions in

the matrix solid solution enriched in solute atoms. Small solute-enriched regions in a solid solution where the lattice is identical or somewhat perturbed from that of the solid solution are called Guinier-Preston zones (G.P. Zones).

2.4 Precipitation in Al-Cu alloys

In aluminum-2 atom percent copper, four different precipitates occur and each may be made to form by controlling the heat treatment. The occurrence of metastable precipitates is quite common in precipitation-hardening alloys. Typical system for describing in details the sequence of events is aluminum-copper although the phenomena mentioned here occur in many other systems.

Guinier-Preston zones of the first kind (GP-I) are plates of copper atoms one or two atoms thick and commonly 25 atoms in diameter oriented parallel to {100} planes in the aluminum-rich matrix. Since the sizes of copper and aluminum atoms differ by about 12 per cent, the lattice is distorted in the regions of the zones. As a matter of fact, the zones here form as thin platelets to minimize strain energy. They form parallel to {100} because the elastic modulus is least in this direction. GP-I forms at room temperature and is the first precipitate to form at 100°C. It is not stable at 210°C; GP-1 formed at a lower temperature rapidly dissolves in about 30 seconded if the metal is heated to 210°C. This is called reversion or retrogression.

Guinier-Preston zones of the second kind (GP-II) are thicker (10 atoms) and of larger diameter (75 atoms) than GP-I, but they are not just big GP-I precipitates. In GP-II an ordering of aluminum and copper atoms occurs to give an average composition of about Cu_2Al_5. GP-II is the second precipitate to form at, say, 130°C or the first at 210°C. The strongest aluminum-2 atom percent copper at room temperature contains mainly GP-II.

θ´ is a third metastable precipitate. It has the nominal composition $CuAl_2$ and is tetragonal with a lattice distorted from θ so that it may form nearly coherently or epitaxially with the aluminum-rich matrix. It forms in the matrix in a Widmenstatten

pattern. The arrangements of atoms in the interface or habit plane are nearly identical in θ´ and the matrix. θ´ begins to form later than GP-II at 130 or 210°C.

Actually all types of precipitates may give hardening but GP zones and ordinary precipitates with some degree of coherency give greater hardening. In some systems, maximum precipitate on hardening occurs with GP zones (aluminum-copper and aluminum-zinc); in some systems maximum hardening occurs with a coherent ordinary precipitate (nickel-titanium, aluminum; nickel, chromium-titanium, aluminum; and aluminum-silver).

Guinier divides GP zones into two classes: ideal and non-ideal. The atomic sizes of zinc and silver differ little from that of aluminum. With these, the lattice of the aluminum-rich matrix is not distorted very much in the region of the zones, which are spherical in shape. These are classed as ideal zones. The zones in aluminum-copper are an example of non-ideal zones.

An important consideration is why metastable precipitates such as GP zones and θ´ should form at low temperatures, rather than the stable precipitate. The answer lies in the theory of nucleation and diffusion-controlled growth. In these cases a large surface energy exists between the stable phase and the matrix, but the GP zone is a perturbation of the matrix and the surface energy is small, indention is difficult for the former, easy for the latter. Very little diffusion is required to nucleate a GP zone. A large number of small particles are able to form during the quench from the solution-treating temperature and on the subsequent low-temperature precipitation heat treatment. Quenched-in vacancies play an important role in facilitating diffusion.

If extra vacancies are present they may be put in by quenching, irradiation or cold work diffusion processes take place at very low temperatures. Some age-hardening alloys (copper-beryllium) do not develop full hardness unless they are cold-worked before aging. The free energy of the system may, of course, be further lowered if the metastable precipitate is replaced by the stable (or a more stable) precipitate. This occurs if the temperature is raised.

2.5 Interaction of dislocation and precipitate

Discussion about the various precipitates in aluminum-copper showed that the problem which must be considered to understand precipitation hardening is the interaction of a dislocation with a field of obstacles. The obstacles of primary interest here are precipitates defined broadly to include Guinier-Preston zones and metastable second phases as well as stable phases.

Consider a row of such obstacles and a dislocation moving on a slip plane. For slip to occur, the dislocation must either move around the particles or through the particles. An active dislocation will select from the various paths available to it the path where the least energy is expanded.

The dislocation may avoid the particles or obstacles by leaving the slip plane in the vicinity of each particle, or it may avoid the particles by the Orowan mechanism [9]. In this mechanism, the dislocation bends between the particles leaving a dislocation ring about each particle. In either case, energy must be supplied to increase the total length of dislocation line.If the Burgers vector for the dislocations is b, the increase in shear stress (τ) over the value for the metal without precipitates, due to bowing of dislocations of line tension T_l between particles of mean planar spacing λ is given by the Orowan equation

$$\tau = 2T_l / \lambda b$$

The significance of this relationship is that anything that increases the inter-particle spacing λ, will rapidly reduce the strength of heat treated alloy.

2.6 Factors that Influence Overaging

2.6.1 Temperature

Increasing temperature can increase the rate of diffusion which may accelerate the dissolution and growth rates and therefore enhance particle coarsening. With increasing

temperature, the maximum solute solubility in the matrix also increases and precipitates may dissolve to release solute in solid solution. Both these mechanisms increase the interparticle spacing and this in turn can soften the alloy.

2.6.2 Diffusion coefficient

During coarsening, solute has to be transported from the dissolving phases to the growing phases. Faster diffusion species accelerate coarsening and the reverse is true for slower diffusing species.

2.6.3 Size of precipitates

Smaller precipitates dissolve faster compared to larger ones. Therefore, the contribution of dislocation-particle interaction to strengthening is lost faster with smaller particles compared to larger ones.

CHAPTER – 3

CASTING PROCESS

Fabrication processes are used to shape, machine and join metals. The metal which is operated is in the form of an ingot obtained by reducing or refining the metal ore. The fabrication processes are basically casting, forging, metal machining, metal joining and finishing. Fabrication of parts with other methods is time consuming. Casting is a fast way to produce the desired shape.

A casting may be defined as a ***"metal object obtained by allowing molten metal to solidify in a mould ",*** the shape of the object being determined by the shape of the mould cavity.

3.1 Advantages of casting process

Certain advantages are inherent in the metal casting process. These often form the basis for choosing casting over other shaping processes such as machining, forging, welding, stamping, rolling, extruding, etc. Some of the reasons for the success of the casting process are:

1. The most intricate of shapes, both external and internal, may be cast. As a result, many other operations, such as machining, forging, and welding, can be minimized or eliminated.
2. Because of their physical properties, some metals can only be cast to shape since they cannot be hot-worked into bars, rods, plates, or other shapes from ingot form as a preliminary to other processing.
3. Construction may be simplified. Objects may be cast in a single piece which would otherwise require assembly of several pieces if made by other methods.
4. Metal casting is a process highly adaptable to the requirements of mass production. Large numbers of a given casting may be produced very rapidly. For

example, in the automotive industry hundreds of thousands of cast engine blocks and transmission cases are produced each year.

5. Extremely large, heavy metal objects may be cast when they would be difficult or economically impossible to produce otherwise. Large pump housing, valves, and hydroelectric plant parts weighing up to 200 tons illustrate this advantage of the casting process.
6. Some engineering properties are obtained more favorably in cast metals. Examples are:

   a) More uniform properties from a directional standpoint; i.e., cast metals exhibit the same properties regardless of which direction is selected for the test piece relative to the original casting. This is not generally true for wrought metals.

   b) Strength and lightness in certain light metal alloys, which can be produced only as castings.

   c) Good bearing qualities are obtained in casting metals.
7. A decided economic advantage may exist as a result of any one or a combination of points mentioned above. The price and sale factor is a dominant one which continually weighs the advantages and limitations of process used in a competitive of enterprise.

There are many more advantages to the metal-casting process; of course it is also true that conditions may exist where the casting process must give way to other methods of manufacture, when other processes may be more efficient. For example, machining procedures smooth surfaces and dimensional accuracy not obtainable in any other way; forging aids in developing the ultimate of fiber strength and toughness in steel; welding provides a convenient method of joining or fabricating wrought or cast products into more complex structures; and stamping produces lightweight sheet metal parts. Thus the engineer may select from a number of metal processing methods that one or combination, which is most suited to the needs of his work.

3.2 Basic steps of casting

Three steps are involved in a casting process[10]:

1) heating metal till it becomes molten
2) pouring the molten metal into a mould
3) allowing the metal to cool and solidify in the shape of the mould.

Casting is used in the automobile industry to produce engine blocks or cylinder heads. Metal casting is vital to our economy and security. Different metals are cast by many different processes for different applications. Cast metal products and processes offer advantages unavailable from products made by other metal forming and fabricating techniques.

Castings are used in areas like transportation, aerospace, defense, mining, construction, maritime, fluid power, & domestic household. Some cast components include: engine blocks, suspension parts for automobiles & fluid flow components like valves, pumps, pipes, and fittings. To cut the emissions there is a need to improve the fuel efficiency and make the vehicle lighter in weight. Non ferrous metal like aluminium is lighter than steel and has density one third of that of steel. Aluminium has a lower density of 2.7 gm/cc compared to 7.8 gm/cc of steel. Aluminum and aluminum alloys are lightweight with good corrosion resistance, ductility and strength.

Aluminium castings are more expensive than ferrous based castings. The greater use of aluminum can decrease vehicle weight, improve its performance and reduce fuel costs. Pure aluminium possesses relatively poor casting features and for this reason castings are prepared from aluminium alloys. The main alloying elements are silicon, copper, magnesium, zinc, etc. Aluminium silicon alloys have good casting and corrosion resistance properties. The fluidity increases with silicon addition. The addition of copper to aluminium increases its strength and hardness. The aluminium copper alloys are heat treatable and possess good machinability.

CHAPTER – 4

LITERATURE REVIEW

Most of the piston alloys used in industries are cast hypereutectic aluminum-silicon alloys. They have some very distinct advantages.

- Light-weight
- Low coefficient of thermal expansion
- low variation

Since the pistons are made to precise tolerances, the manufacturer needs to pour the alloy into the mold and have them solidify exactly the same way every time. An alloy with a composition near its eutectic will solidify almost all at once. An alloy that has a composition far from its eutectic will solidify at different rates with regard to the parts of each of the alloying elements. The precipitations of a hypereutectic alloy of Al-Si are an example of this but are tightly controlled to gain the desired properties and maintain low variation from one cast piston to another.

These advantages come from the properties of the hypereutectic alloy used. Thus, considering this fact that these exhibit good bearing properties, we have selected alloys of near eutectic composition but of hyper side.

4.1 Al-Si eutectic composition

Aluminum silicon foundry alloys are usually alloyed close to the eutectic or near eutectic compositions due to the small freezing range, good castability and desirable properties obtained at these compositions. As the molten alloy is cooled the silicon begins to come out of solution and form precipitates. Some of the silicon remains undissolvd in the matrix of aluminium. These little "islands" of silicon that are spread throughout the aluminum matrix greatly harden the metal and create a phenomenon known as

precipitation hardening. They also cause a change in thermal properties resulting in a lower coefficient of thermal expansion and heat transfer.

Understanding the mechanism by which the eutectic forms and grows is important. During the solidification of aluminum silicon alloys, first the primary dendrites grow. After the dendrites impinge upon each other, the dendrite mobility is restricted. Mass transport to compensate for shrinkage occurs mainly by interdendritic feeding. Interdendritic feeding involves the flow of eutectic liquid. Thus, the origin and growth of the eutectic is of major importance to fluid flow.

Figure 4.1 shows the microstructure of the aluminum-silicon eutectic. In general, when there are approximately equal volume fractions of the two phases, eutectics of binary alloys exhibit a lamellar structure. On the other hand, if one phase is present in a small volume fraction, this phase tends to be fibrous. As a rule of thumb, the eutectic microstructure obtained will tend to be fibrous when the volume fraction of the minor phase is less than 0.25, otherwise it will tend to be lamellar [11]. If both phases in the eutectic are non-faceted, the eutectic will exhibit a regular morphology. In this case, the microstructure is made up of either lamellae or fibers having a high degree of regularity and periodicity.

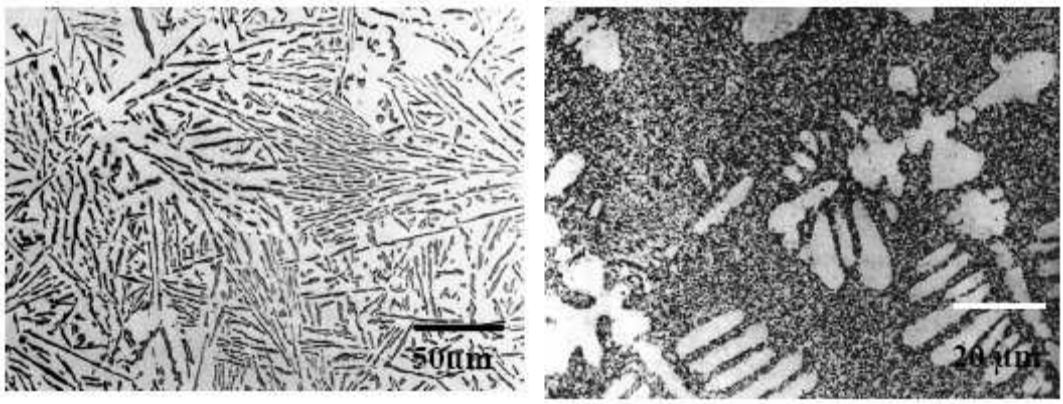

Figure 4.1: Al-12.5wt% Si alloy (a) Slowly cooled 200X (b) Chill Cast 500X

On the other hand, if one phase is faceted, the eutectic morphology is often irregular. Even though the volume fraction of silicon in the aluminum-silicon binary is less than

0.25, the typical aluminum-silicon eutectic is closer to a lamellar structure than to a fibrous one. This is usually attributed to the strong anisotropy of growth of silicon and to the relatively low interfacial energy between silicon and aluminium.

Primary silicon is the pre-eutectic silicon formed in hypereutectic aluminum-silicon alloys. Primary silicon tends to assume different morphologies like massive crystals of geometric star like or dendritic shape, complex regular silicon morphology. At higher growth velocities, the edges and corners become the preferred growth sites, leading to the formation of dendritic type silicon phase as shown in Figure 4.2. Higher growth velocities cause isotropic growth of silicon resulting in the formation of dendritic morphology as in metals.

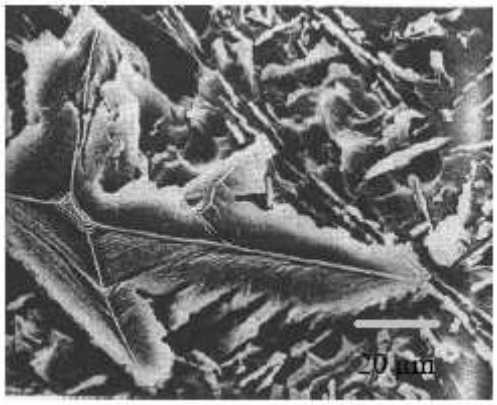

Figure 4.2: Dendritic primary silicon in Al-17%Si.

4.2 Modification of silicon by addition of different elements

Addition of some elements like sodium or strontium in trace amounts causes a change in the solidification, morphological characteristics of silicon both in eutectic and primary form. This change (specifically the morphological change) is termed as modification. Because of its commercial importance, study of this phenomenon of modification has been the subject of intense research efforts dating back to early 1920s till today. In this section, the various changes associated with modification and different theories explaining these changes are reviewed. Sodium was used predominantly as the modifier till the late 70s, after which strontium was used.

Modification of the Al–Si eutectic from a flake-like to a fine fibrous silicon structure can be achieved in two different ways; by addition of certain elements (chemical modification) or with a rapid cooling rate (quench modification). Several elements are known to cause chemical modification. The most common elements used in industry today are Sr and Na, which changes silicon from coarse plate-like to a fine fibrous structure, and Sb which only causes a refinement in the plate-like silicon structure. Addition of other alkali, alkaline earth and rare earth metals have also been reported to cause modification, although very limited data is available in the literature.

The variation in structural features for the two Al-Si alloys both of composition 13wt% Si when doped and undoped with small degree. The two alloys are Al-13wt%Si and Al-13wt%Si-0.01%Na. As this alloy is hypereutectic, primary Si forms first, depleting the liquid of Si until it reaches the eutectic composition where the remaining solidification follows the eutectic reaction. The primary Si has a cuboidal form which can be seen in the micrograph figure4.3. The eutectic mixture, though, is non-lamellar in form and appears, in section, to consist of separate interconnected flakes (Figure 4.3 (a)). Adding a small quantity of a ternary element, here sodium, causes modification in the microstructure. This addition effectively moves the eutectic point to a higher silicon concentration and lower temperature. This modifies the growth of the eutectic silicon to produce an irregular fibrous form rather than the usual flakes.

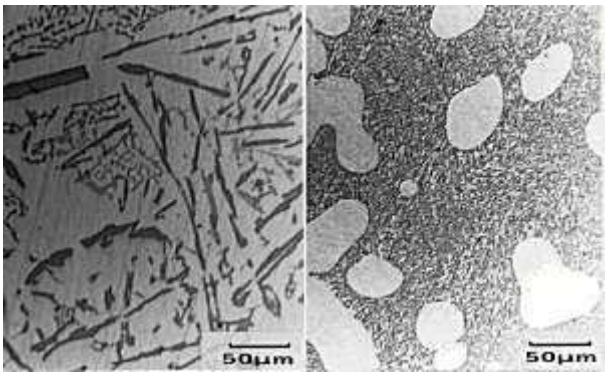

(a) (b)

Figure4.3: Micrograph of (a) un-doped and (b) Na doped alloy.

The eutectic point has moved far enough to make the alloy, at this composition, hypo-eutectic instead of hyper-eutectic. So now primary alpha forms, rather than primary Si. White blobs of primary alpha dendrites can be seen, surrounded by a fine, fibrous eutectic mixture of alpha and Si figure4.3 (b).

Major [12] conducted directional solidification experiments with and without strontium. Platelet morphology of silicon in low growth rate, changes into a massive irregular silicon phase. Figure 4.4(a) shows the unmodified silicon, followed by modified silicon in Figure 4.4(b).

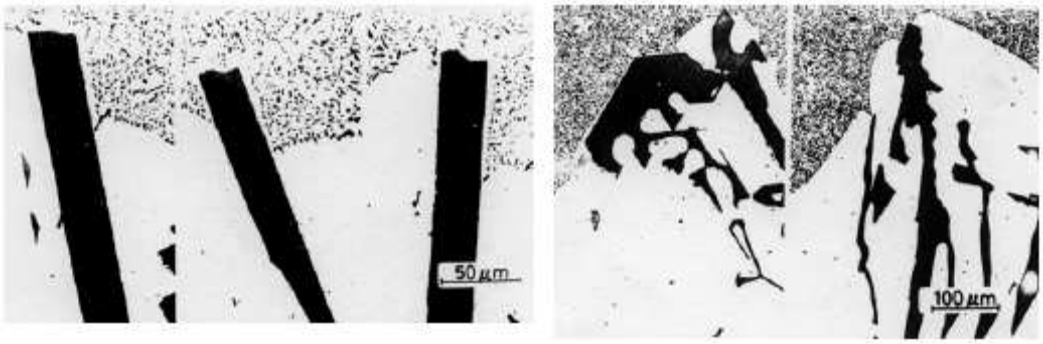

Figure 4.4: (a) Unmodified aluminum silicon eutectic in with the quench interface (b) Modified aluminum silicon eutectic (0.3%Sr) with the quench inte--rface.

A. Knuutinen, K. Nogita, S.D. McDonald, A.K. Dahle [13] studied the modification of Al–Si alloys with Ba, Ca, Y and Yb. Modification of Al–Si alloys is known to result in a depression of the eutectic arrest temperature. It has been suggested that a larger depression is related to increased modification. The effects of different concentrations of separate additions of Ba, Ca, Y and Yb on the eutectic arrest in an A356.0 (Al–7%Si–Mg) alloy have been studied by thermal analysis. All of these elements cause a depression of the eutectic arrest, however Ba and Ca result in fibrous eutectic Si while Y and Yb result in a refined plate-like eutectic silicon. Analysis of the effects of the elements on eutectic nucleation and growth temperatures and the recalescence shows two different trends. Addition of Ba and Yb both causes linear changes with increased concentration, while addition of Ca and Y result in an instantaneous effect with the first addition and no further significant changes with increased concentration.

An assembly of all cooling curves collected for different barium contents is shown in Figure 4.5. The scale of the figure 4.5 is adapted to best illustrate the behaviour around the eutectic arrest and the time scale is such that it does not cause any overlap of the cooling curves. Corresponding micrographs of a representative eutectic region in each sample are also shown.

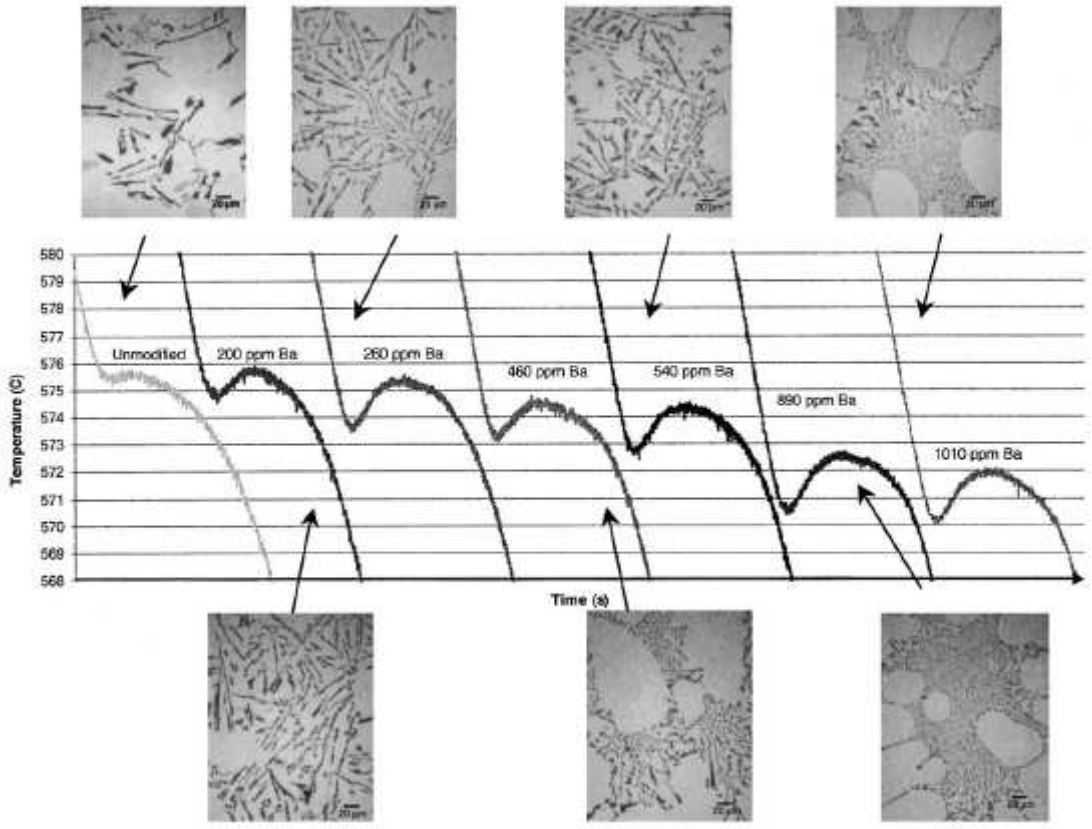

Figure 4.5: Assembly of cooling curves, with focus on the eutectic reaction, for all tested Ba addition levels to the A356.0 alloy with corresponding optical micrographs of representative eutectic structure in each sample.

A coarse plate-like silicon morphology was observed at barium levels of 200 and 260 ppm. The microstructure is similar to that in the unmodified alloy without significant modification. Several regions of very refined, fibrous, silicon were observed with addition of 460 ppm Ba. The eutectic was fully modified at 890 ppm Ba, i.e. with a fine fibrous eutectic across the sample. Further barium additions resulted in an increasingly

refined eutectic structure. It should be noted that large blocky particles were observed in the microstructure for barium levels exceeding 500 ppm.

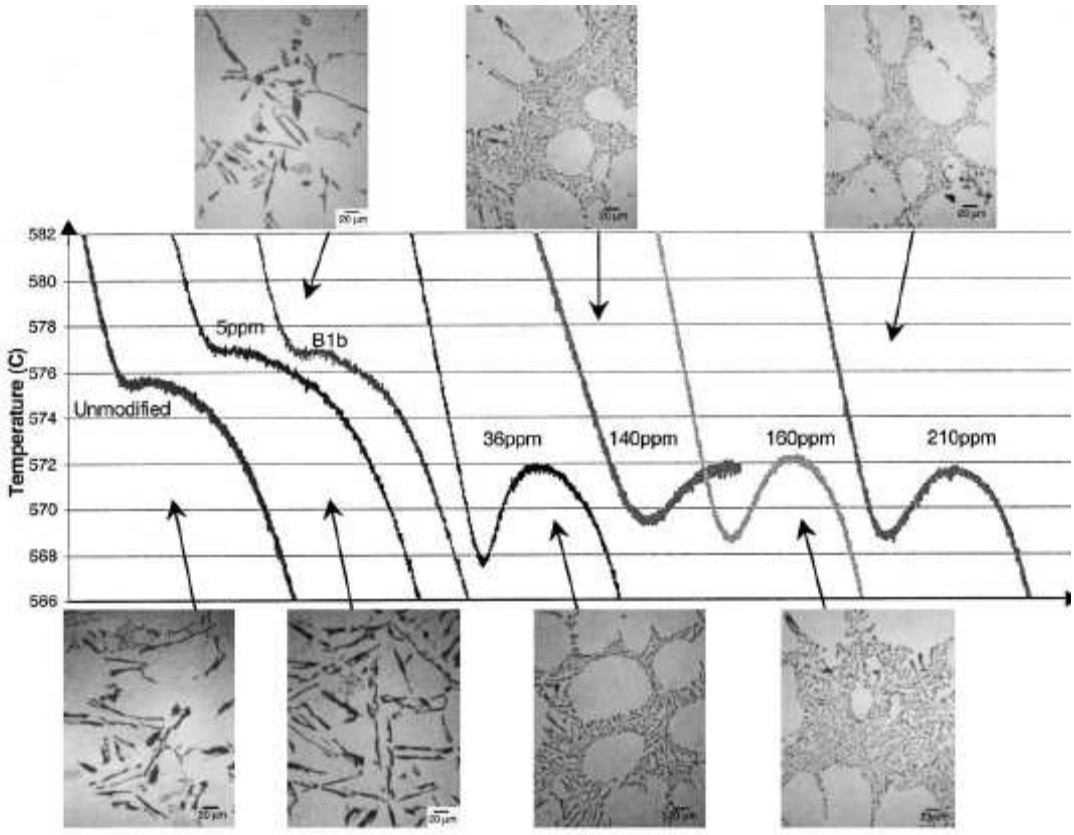

Figure 4.6: Assembly of cooling curves, with focus on the eutectic reaction, for all tested Ca addition levels to the A356.0 alloy with corresponding optical micrographs of representative eutectic structure in each sample.

It can be clearly observed in Figure 4.6 that the first addition of Ca, 36 ppm, causes a large change in the cooling curve compared to the unmodified alloy. The growth temperature has dropped about 4°C and a large recalescence effect is observed prior to the eutectic arrest. The corresponding microstructure contains wellmodified fibrous silicon. Further increases in calcium content do not seem to alter the cooling curves significantly, i.e. the eutectic growth temperature and recalescence seems largely unaffected, and the eutectic microstructure remains well-modified and does not change significantly with increased calcium content.

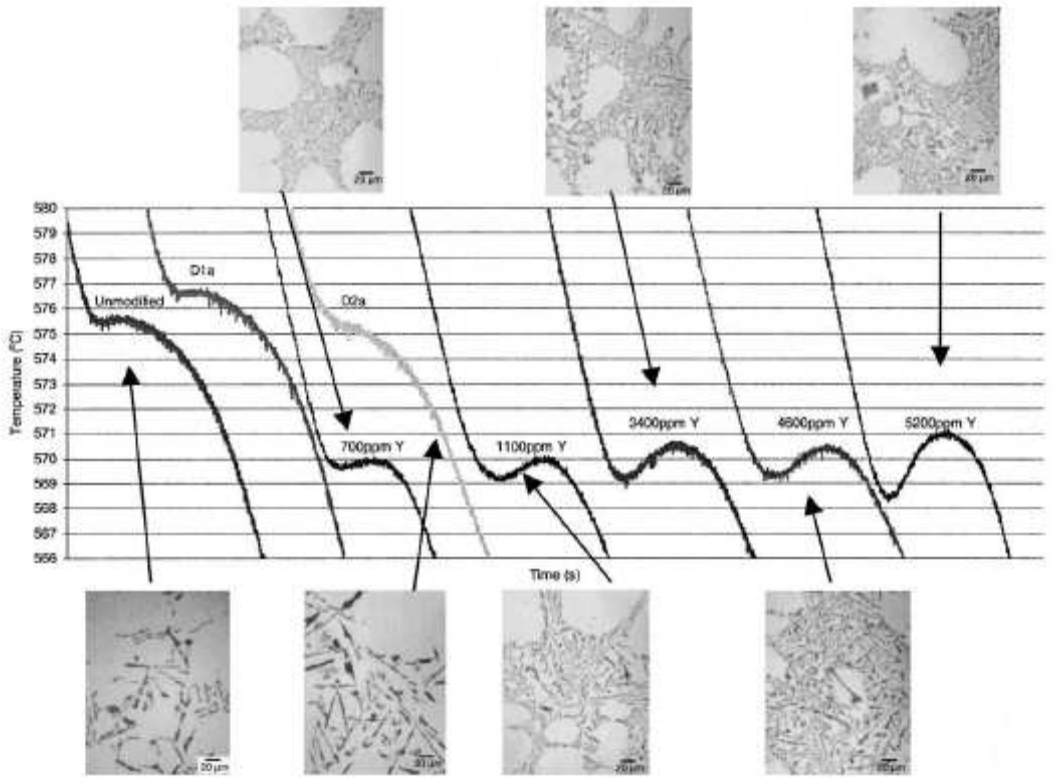

Figure 4.7: Assembly of cooling curves, with focus on the eutectic reaction, for all tested Y addition levels to the A356.0 alloy with corresponding optical micrographs of representative eutectic structure in each sample.

In Figure 4.7 the cooling curve and microstructure of the unmodified base alloy is also shown. The cooling curves have been offset along the time scale to assist the comparison of the eutectic arrests. It is readily apparent from Figure 4.7 that the addition of yttrium causes a significant depression of the eutectic arrest. The recalescence increases continuously with increasing yttrium concentration, while the eutectic growth temperature first decreases significantly with the introduction of 700 ppm Y and then seems to show a slight increase with further increases in yttrium content. The micrographs show that yttrium causes modification of the silicon to a refined plate-like structure and the level of refinement of the silicon seems relatively constant as the yttrium content is increased from 700 to 5200 ppm. A new phase was observed in the microstructure at the higher levels of yttrium addition.

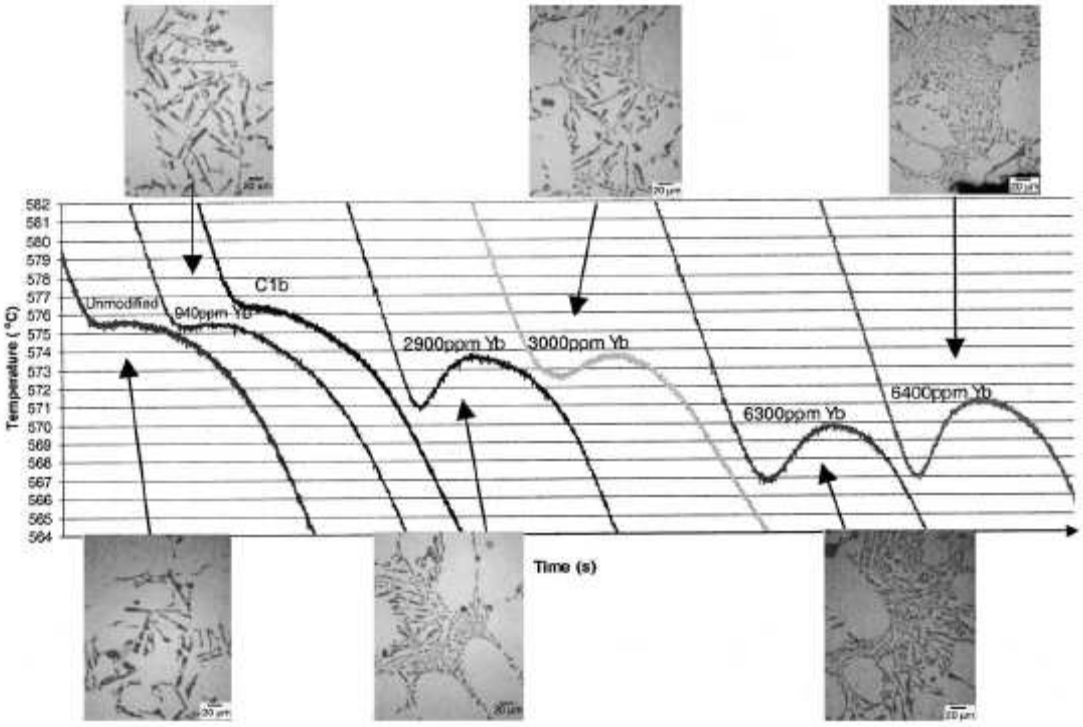

Figure 4.8: Assembly of cooling curves, with focus on the eutectic reaction, for all tested Yb addition levels to the A356.0 alloy with corresponding optical micrographs of representative eutectic structure in each sample

Figure 4.8 shows an assembly of the cooling curves with focus on the eutectic arrest for all ytterbium levels investigated in this work. The cooling curve for the unmodified alloy is also shown. Representative micrographs of the eutectic microstructure are shown for each sample. It should be noted that the cooling curves have been offset along the abscissa to ease the comparison. With addition of 940 ppm ytterbium the eutectic is very coarse and flake-like, similar to the unmodified alloy. When the ytterbium content is increased to 2900 ppm the eutectic silicon is still plate-like, but much refined compared to the unmodified alloy, and the sample was only partly modified. A modified fine plate-like structure is observed across the whole sample at 6300 ppm Yb.

Chang J., Moon I. and Choi C [14] studied the refinement of cast microstructure of hypereutectic Al-Si alloys through the addition of rare earth metals.they performed the microstructural observation and thermal analysis of Al-21 wt % Si alloys with different rare earth metals to examine the effect of rare earth metal on the refinement of primary silicon phase. Simultaneous refinement of both primary and eutectic silicon morphology

is achieved with the addition of rare earth and its effect increases with the amount of rare earth addition and cooling rate. Depression of 12–17 °C in primary reaction temperature and 2–7 °C in eutectic temperature is measured with the addition of rare earth. Rare earth bearing compounds were not believed to act as a nucleation agent of primary silicon phase. Some rare earth bearing compounds determined to AlCe were around primary silicon in the matrix. The twin density of eutectic silicon remains same regardless of the addition of rare earth. The refinement of silicon in rare earth treated hypereutectic Al-Si alloys is supposed to be due to the suppression of the nucleation temperature of silicon phase.

4.3 Mechanical properties

Rajesh Sharma, Anesh Kumar and D.K. Dwivedi [15] studied the influence of solution temperature 450-550°C on microstructure and mechanical properties of cast Al-12% Si-0.3% Mg and Al-16% Si-0.3% Mg alloys has been reported. It was observed that an increase in solution temperature increased the tensile strength of all alloys under investigation. Ductility was adversely affected. Higher solution temperature produced better refinement and distribution of eutectic silicon crystals than a low temperature. Heat treatment of all alloys showed spheroidization of eutectic silicon crystals. Scanning electron microscopy (SEM) of tensile-fractured surfaces was carried out to investigate the influence of solution temperature on the mode of fracture.

Li Rong-de, Li Run-xia, Yu Li and Hu Zhuang-qi [16] investigated the effect of trace elements Cd and Sn on the microstructure and mechanical properties of Al-Si-Cu-Mg cast alloy. With the increase of Cd addition the strength of alloy rises at first and then drops. The optimal amount of Cd and Sn addition for Al-Si-Cu-Mg alloy is about 0.27% and 0.1% respectively. Due to the formation of some coarse Cd-rich phases and pure Cd particles the mechanical properties of alloy decrease when Cd amount exceeds 0.27%. When more than 0.1% Sn added, some Sn atoms form low-melting eutectic compound at grain boundary, and then cause over-burning in alloy when solution treated, which may deteriorate properties of alloy, especially ductility of alloy. On the other hand, the

addition of Cd and Sn remarkably increases the peak hardness and reduces the time to reach aging peak in Al-Si-Cu-Mg alloy. The action of Cd/Sn in quaternary Al-Si-Cu-Mg alloy is effectively the same as that occur in binary Al-Cu alloy that the enhanced hardening associated with Cd/Sn addition is due to the promotion of the θ' phase.

M.F. Moreira and R. Fuoco [17] have done the study of characteristics of fatigue fractures in Al-Si cast components. As introduction, the general aspects of fatigue fractography and some examples of fatigue failures in aluminum cast components are presented. The examples of fatigue failures emphasize the microfractographics aspects and their relationship with microstructures of alloys. The three stages of fatigue are directly related to the macrographic aspects of the fatigue fractures. The process of fatigue consists of three stages [18]:

- Crack initiation (stage I)
- Progressive ("stable") crack growth across the component (stage II)
- Final sudden fracture of the remaining cross section of the component (stage III)

The microstructures of cast Al-Si alloys is essentially constituted by dendrites of α-phase, eutectic cells of α + Si and tertiary eutectics (iron rich, magnesium rich and copper rich eutectics) precipitated in the intercellular regions. Since all these second phases (Si, $CuAl_2$, Mg_2Si, Al_5FeSi and $Al_{15}(Fe, Mn)_3Si_2$) are harder than the α phase, if the localized stress level surpasses the material yield strength, there will be some deformation of the α-phase matrix while the hard phases may fracture or experience some decohesion from the α-phase matrix, thus forming microvoids. In the absence of stress concentration factors, the second phase decohesion from the α-phase matrix or the crack of the second phase can be the fatigue crack nucleation event (stage I). The morphology and the size of the second phases in the microstructure of the Al-Si alloys are important factors causing stress concentration in the α-phase matrix around them. Rounded and small second phases particles cause lower stress concentration levels and delay the fatigue crack nucleation. Rounded and small Si particles can be attained by good modification treatment practice and rapid solidification rates (permanent mold).

Additionally, the solution heat treatment contributes to the breakdown and coalescence of the Si particles.

Although these technical aspects are well known for components subjected to fatigue, overmodification problems are very frequently observed. Figure4.9 presents microstructures of A356 alloy in three different conditions: without modification, with Sr-modification + heat treatment and with Sr-overmodication + heat treatment. Also, changes in the morphology of the Si particles obtained by means of the modification treatment and solution heat treatment reduces the fatigue crack propagation rate in stage II [19].

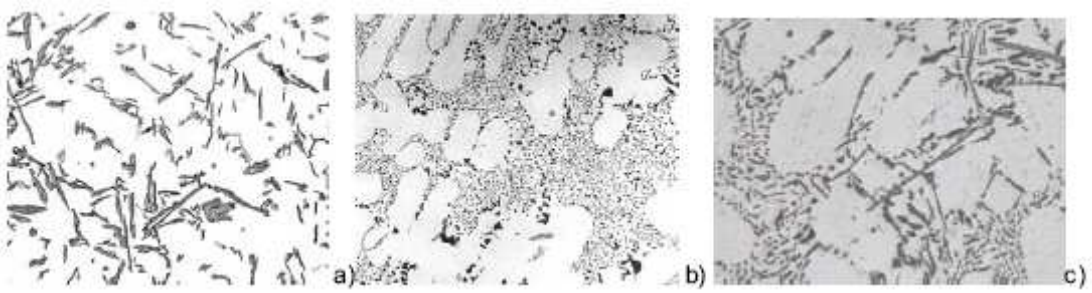

Figure 4.9: Microstructures of A356 alloy in three different conditions: a) without modification (200X); b) with Sr-modification + heat treatment (200X) and c) with Sr-overmodication + heat treatment (200X).

At the same time, there is no practical solution to control the morphology of the other second phases ($CuAl_2$, Mg_2Si, Al_5FeSi and $Al_{15}(Fe, Mn)_3Si_2$), so the common practice is to minimize the copper and iron contents to reduce the fraction of second phases and to apply high solidification rates, in order to obtain smaller particles. Certainly, much more important to the stress concentration and to fatigue crack nucleation (stage I) is the presence of casting defects as microporosities, oxide inclusions and shrinkage porosities, since the sizes of these defects are much larger than the size of the microstructure particles. The reduction of the fatigue life of the component is directly proportional to the casting defect size [19, 20].

Figure 4.10a presents the aspect of a diesel engine manifold, which failed in field after 200,000km. The crack is coincident with a reentrant sharp angle. The part was produced in 11%Si-0.22%Mg-0.36%Fe-0.25Mn with Na-modified alloy using sand mold. Figure 4.10b shows the typical microstructure of the casting with α-phase dendrites and α+Si eutectic, with modified Si particles, and the presence of some iron-rich phase, probably, $Al_{15}(Fe, Mn)_3Si_2$. There are numerous large sized microporosities. The general aspect of the fatigue fracture surface is presented in Figure 4.10c. Although, the component failed in field, there is no evidence of beach marks suggesting that the load cycles during the component life were essentially constant. Examination of the fatigue fracture surface in SEM shows the presence of fatigue striation, as presented in Figure 4.10d. The possible explanation for the short fatigue life of the component is the component design (sharp corner) associated to the large size and high amount of microporosities.

Figure 4.11 a and 4.11b present a fatigue fracture in the head of an automotive diesel engine piston cast using 339 alloy with 13 % Si. The fatigue fracture surface exhibits the traditional beach marks (Figure 4.11c). The microstructure is constituted mainly by primary Si particles, α + Si main eutectic and secondary eutectics of Cu, Mg and Fe, with no α dendrites. The microstructure and the low magnification SEM aspects are presented in Figure 4.11d and 4.11e, respectively**.** In contrasts with the previous examples, there is no evidence of smooth region in the stage II region of the fatigue fracture surface. Also, the fracture surface presents a ratchet mark in the crack propagation direction, probably as a consequence of two independent fatigue crack propagation in parallel direction, which tend to unification. Observations in SEM with high magnification, hardly characterize the presence of fatigue striation (Figure 4.11f).

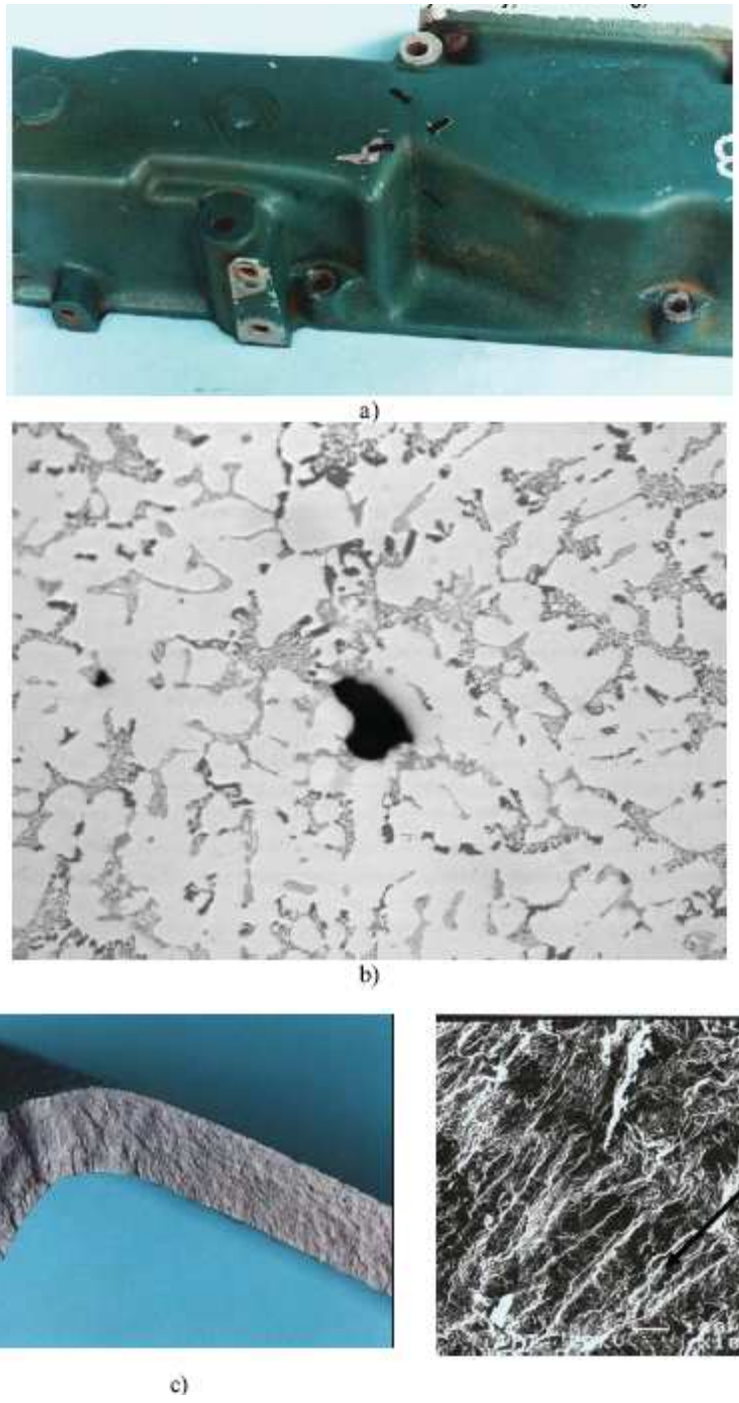

Figure4.10: Fatigue fracture in diesel engine manifold (a) coincident with a reentrant sharp angle; b) microstructure of Al-11%Si with modified Si particles and numerous large sized microporosities; c) aspect of the stage II region of the fatigue fracture surface; d) tear ridges in the fatigue crack propagation direction, as observed in SEM.

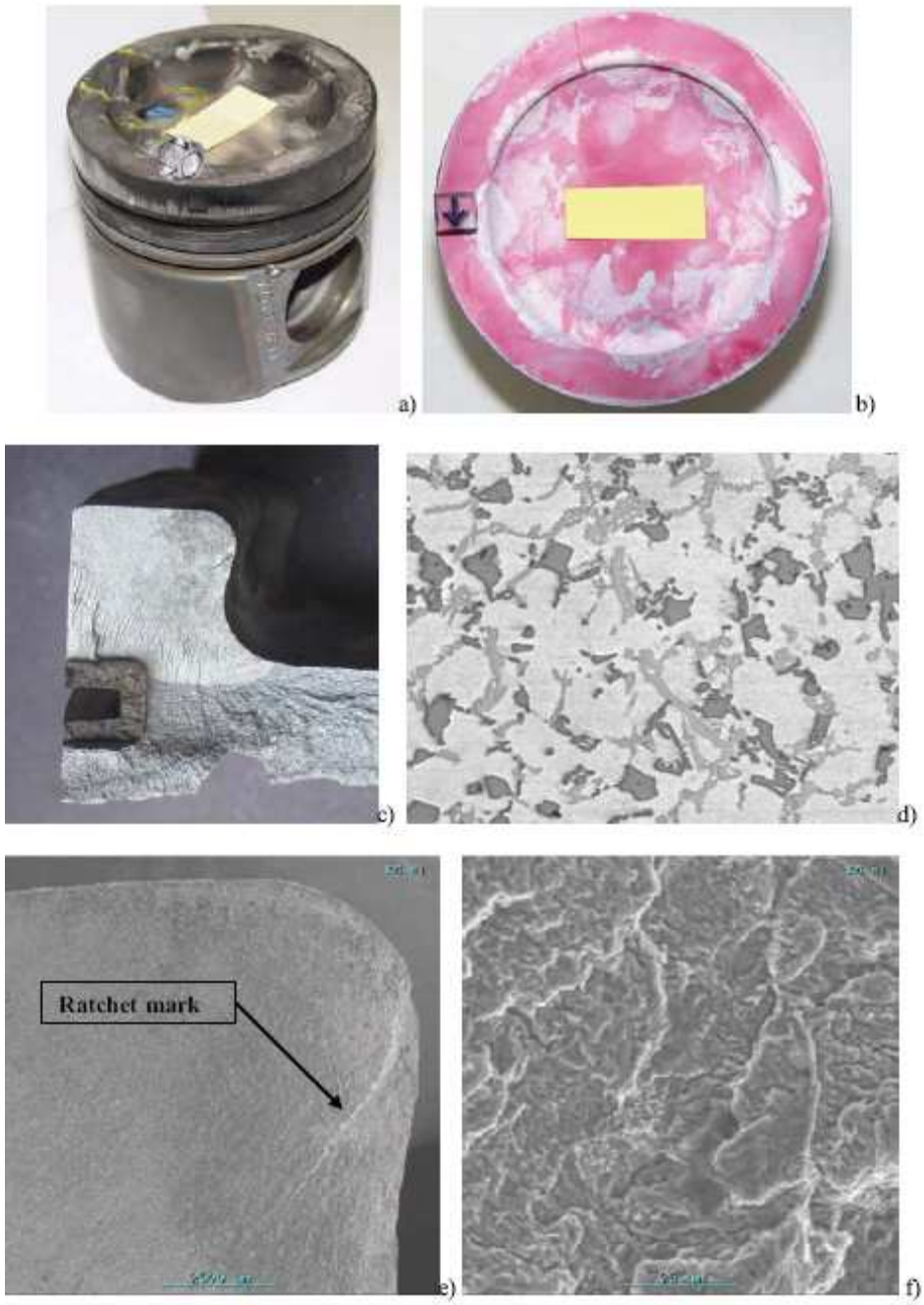

Figure 4.11: General aspect of an automotive diesel engine piston cast using 339 alloy with 13%Si (a), which presents a fatigue crack (b) in the head region; c) aspect of the fatigue fracture surface presenting beach marks; d) microstructure of the 339 alloy constituted mainly by primary Si particles, α + Si main eutectic, without α dendrites; e) SEM low magnification image of the fatigue fracture surface, without evidence of smooth region. There is a ratchet mark in the crack propagation direction; f) high magnification SEM observation: fatigue striations are barely seen.

It was concluded with the study of different Al-Si alloys that:

- The main macrographic characteristic of the fatigue fracture of Al-Si cast components is the presence of beach marks concentric in relation to the crack initiation region;
- The main micrographic characteristics of the fatigue fracture in Al-Si cast components are the tear ridges in the direction of the crack propagation and the fatigue striation in a direction perpendicular to the crack propagation;
- The presence of the fatigue striation is easily observed in the regions of α dendrites and hardly observed in eutectic regions, so the detection of fatigue striation in Al-Si cast components depends on the α dendrites content in the microstructure.

S.P. Nikanorov [21] studied structural and mechanical properties of Al–Si alloys obtained by fast cooling of a levitated melt. The aim of his work was to determine the structure and mechanical properties of near eutectic and hypereutectic Al–Si alloys with high Si content obtained by fast cooling.

Optical microscopy revealed a fine-grained structure for samples prepared by quenching of liquid metal. Figure 4.12 shows the optical micrographs of Al–Si alloys obtained by casting of levitated melts for (a) 11.5, (b) 20, (c) 25, (d) 30 and (e) 35 wt.% Si. In the hypoeutectic alloy (Figure 4.12a) there is eutectic structure with primary crystals of Si solid solution in Al. The 20 wt.% Si alloy (Figure 4.12b) has an anomalous finest-grain eutectic structure. There are star-shaped primary Si crystals on the background of eutectic structure for the 25 wt.% Si composition (Figure 4.12c). The concentration and size of primary Si crystals increase with increasing Si content (30 and 35 wt.% Si).

Figure 4.13 shows that Young's modulus *E* increases with increasing Si content. It is noteworthy that alloys prepared by quenching of the levitated melt had higher *E* values than those obtained with conventional casting.

The Vickers hardness was measured only for samples with Si content up to 15 wt.%. The Vickers hardness of transverse sections was slightly higher for 15 wt.% Si alloy (HV =440 ±10MPa) than for the sections of 11.5 wt.% Si alloy (HV = 430 ±20MPa).

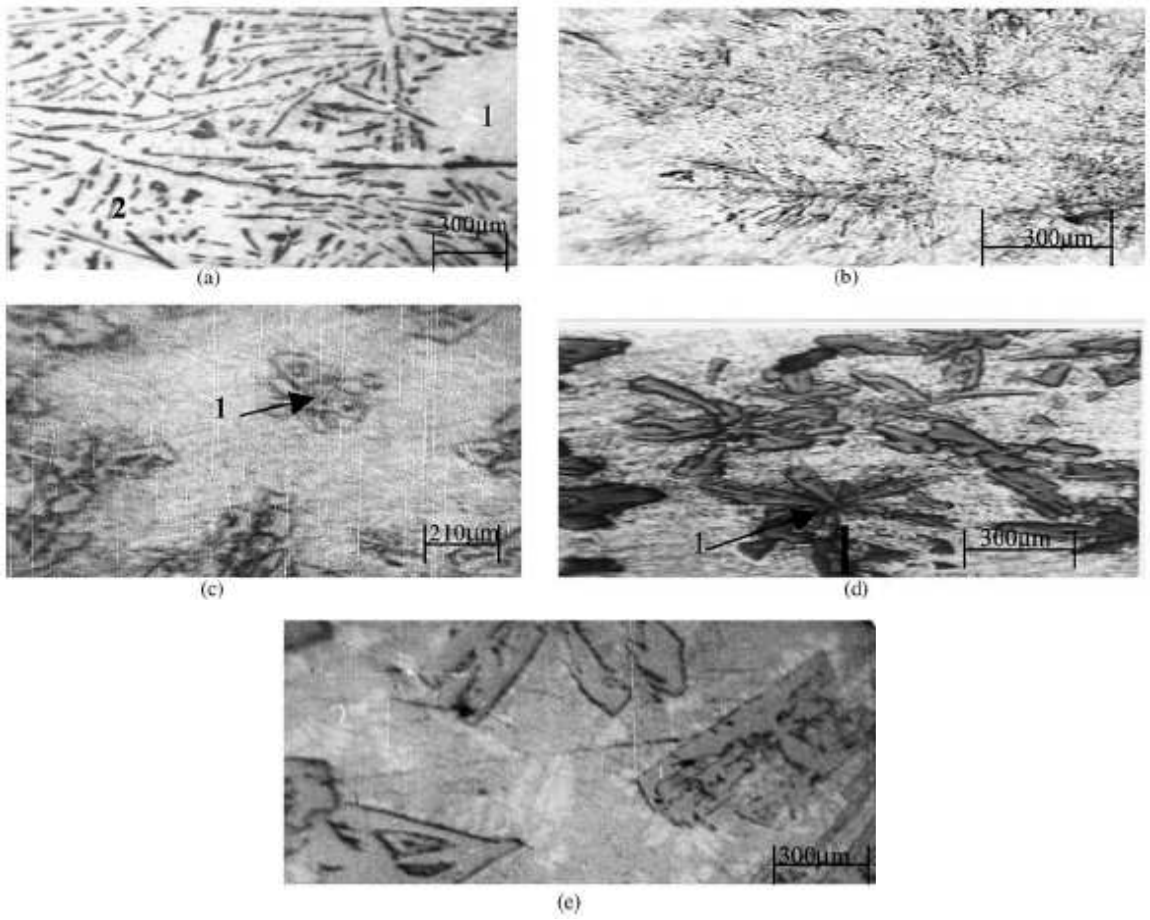

Figure 4.12: Microstructure of Al–Si alloys vs Si content: (a) 11.5 wt.% Si, 1 is the primary crystal of α solid solution, 2 is the eutectic structure with needle like Si component of black colour. (b) 20 wt.% Si. (c) 25 wt.% Si, 1 is star like primary Si crystal. (d) 30 wt.% Si, 1 is star like Si primary crystal. (e) 35 wt.% Si.

Fig. 4.14 shows the temperature dependence of Young's modulus of Al–Si alloys with 11.5, 20, 25 and 30 wt.% Si as well as for Al–11.5 wt.% Si with added 0.01 wt.% Sr. Note that there is temperature hysteresis of Young's modulus for all alloys quenched from the levitated state except for the Al–11.5 wt.% Si–0.01 wt.% Sr alloy. The hysteresis depended on the alloy composition.

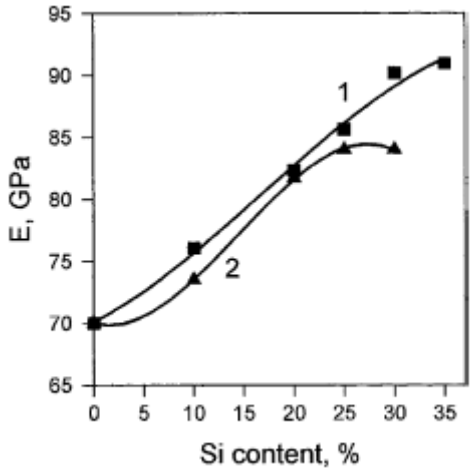

Figure 4.13: Young's modulus of Al–Si alloys vs. Si content at room temperature: (1) present results, (2) the results for conventional casting into a mould.

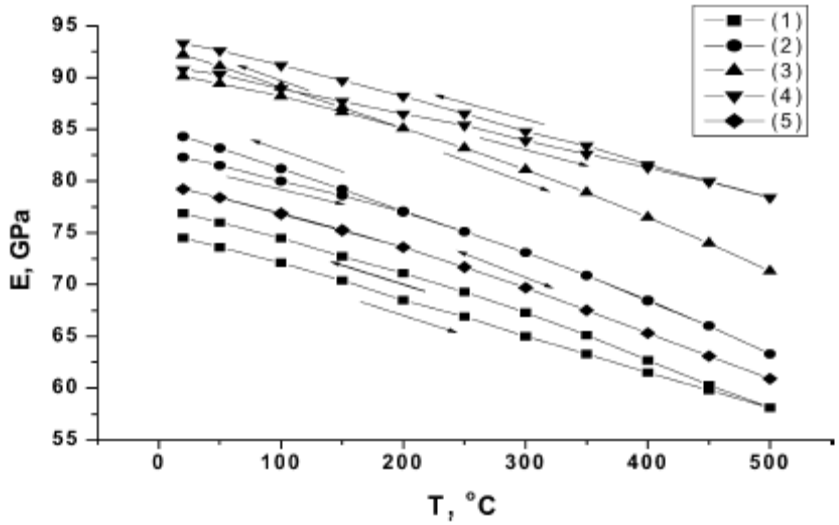

Figure 4.14: Young's modulus of Al–Si alloys vs. temperature for various Si contents: 1—11.5wt.%, 2—20wt.%, 3—30wt.%, 4—35wt.% Si; 5—Al–11.5% wt.% Si–0.01% wt.% Sr.

As shown in Figure 4.15a, the load *P* corresponding to the yield point also exhibits a maximum at about 20 wt.% Si. The Si content corresponding to maximum value of the yield point is higher then for the eutectic point of Al–Si alloy (about 11.7%) that is seen from Figure 4.15b, where high temperate part of the phase diagram of the alloy is shown.

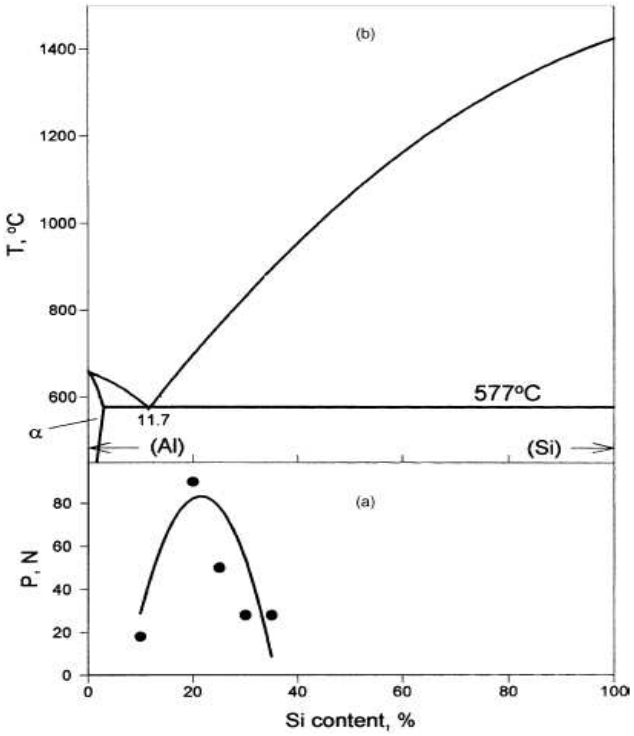

Fig. 4.15: (a) The yield point P as a function Si content. (b) The aluminum–silicon phase diagram (Si content in wt.%).

The mechanical behaviour reported above is related to the microstructure, which can be understood with the help of the diagram of microstructure of Al–Si alloys vs. composition and solidification rate, as determined experimentally in for a Si content up to 17%. Figure 4.16 shows this diagram with the upper border of the region of coupled growth, the region II, extrapolated by us from 17 to 35 wt.% Si. Note that there is a wide range of Si concentrations and solidification rates giving coupled growth of a fine fiber eutectic-like structure without any primary crystals. The solidification rate was estimated to be between 10^3 and 10^4 K/s. In [22, 23] the melt quenching was performed for similar conditions and the measured cooling rate supported our estimated value.

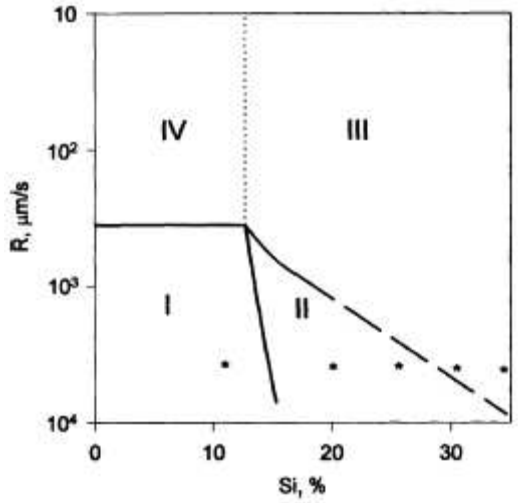

Figure 4.16: Diagram of Al–Si alloys microstructure vs. Si concentration and cooling rate *R*.

The alloys compositions and the approximate solidification rate used in the present work are indicated by star-like points in Figure 4.16. From this figure, it follows that our Al–20 wt.% Si alloy was produced in the region coupled eutectic growth and its finest eutectic-like structure without any primary crystals is responsible for the maximum yield point. The samples of Al–11.5 wt.% Si were obtained outside this region and had a coarser eutectic structure with α dendrites, resulting in lower yield point. The samples of 25 wt.% Si were cast close to the border of the region III and the alloys with 30 and 35 wt.% Si in the region III where primary Si crystals were growing. It is necessary to note that the borders of the regions were shown for 50% transformation of the structures. Therefore the alloys with Si content in the region from 25 to35 wt.% for our the solidification rate should have had inclusions of primary Si crystals, the sizes and numbers of which increased with increasing Si content. The interface between these crystals and the eutectic matrix decreases the yield point. Increasing the Si content is thought to decrease the temperature coefficient of Young's modulus due to increasing covalent contribution to atomic bonding.

In the quenched samples the Si content of α solid solution exceeds the equilibrium value. The Guinier–Preston zones can arise under heating of the samples during these measurements. In the zones with higher Si concentration the contribution of covalent

interatomic forces increases. It causes the increasing of *E* during the heating of samples and decreasing of the temperature coefficient of E. Maximum on the concentration dependence of the temperature coefficient of Young's modulus at 20 °C can be explained by the finest eutectic structure of the alloy making difficult the creation of the zones.

Hengcheng Liao, Yu Sun and Guoxiong Sun [24] studied the correlation between mechanical properties and amount of dendritic α-Al phase in as-cast near-eutectic Al–11.6% Si alloys modified with strontium. The amount of dendritic α-Al phase with varying Sr content in near-eutectic Al–11.6% Si alloy was measured by quantitative metallography analysis software and the correlation of mechanical properties of fully modified alloy with the amount of dendritic α-Al is discussed. Addition of Sr in Al–Si alloys results in a considerable increase of the amount of α-Al. Mechanical properties of the fully modified alloy are linearly related to the volume fraction of dendritic α-Al, which plays a key role in improving the mechanical properties of near-eutectic Al–Si alloys.

The following conclusions can be made from the results of the present investigation.
(a) Addition of 0.0375% Sr to Al–11.6% Si alloy promotes the growth of columnar dendrites and results in a remarkable increase in the amount of dendritic α-Al phase, by 236.9% compared to the unmodified alloy.
(b) When the Sr content increases from 0 to 0.0375%, the ultimate tensile strength and fracture elongation increase by 34.0 and 714.6%, respectively. The quality index, a combination measure of mechanical properties, increases by 100%.
(c) Mechanical properties of the modified alloy are linearly related to the amount of dendritic α-Al phase present. It is suggested that the dendritic α-Al phase plays an important role in improving the mechanical properties of near-eutectic Al–Si alloys.

4.4 Wear characteristics

Feng Wang, Huimin Liu, Yajun Ma and Yuansheng Jin [25] have studied the effect of Si content on the dry sliding wear properties of spray-deposited Al–Si alloy. In their

investigation, Al–12Si, Al–20Si and Al–25Si (wt%) alloys were synthesized by spray atomization and deposition technique. The wear resistance of the alloys was studied using a pin-on-disc machine under four loads, namely 8.9, 17.8, 26.7 and 35.6 N. The microstructures, worn surfaces and the debris were analyzed in a scanning electron microscope. It had been found that the effect of Si content on dry sliding wear of spray-deposited Al–Si alloy was associated with applied loads. At lower load (8.9 N), with increasing Si content, the wear rate of the alloy was decreased. At higher load (35.6 N), spray-deposited Al–20Si alloy exhibited superior wear resistance to the Al-12Si and Al-25Si alloys. Figure 4.17 shows the wear test results, which represent the wear rate as a function of the applied load.

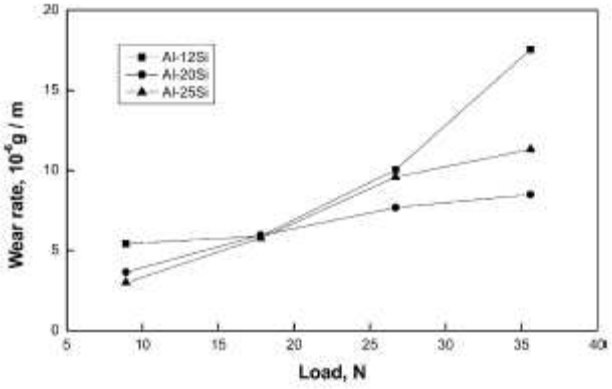

Figure 4.17: Variations in the wear rates of spray-deposited Al–Si alloys with load.

Dheerendra Kumar Dwivedi [26] studied the wear behaviour of cast hypereutectic aluminium silicon alloys. He reported the influence of alloying elements on wear behaviour of binary (Al–17%Si) and multi-component (Al–17Si–0.8Ni–0.6Mg–1.2Cu–0.6Fe) cast hypereutectic aluminium alloys. Experimental alloys were prepared via foundry technique. Wear behaviour of Al–17Si and Al–17Si–X {X = Ni, Cu, Mg, Fe} alloys was studied using pin on disc (ASTM: G99) type of friction and wear testing machine. Dry sliding wear tests were performed at various sliding speeds (0.2–4.0 m/s) and contact loads (10–30 N) against hardened ground steel disc (hardness 60 HRC). It was observed that the addition of alloying element not only reduces the wear rate in mild oxidative wear condition but also increases the transition load. Temperature of wear pin

near the sliding surface was measured and it was related to wear and friction behaviour of experimental alloys. Increase in hardness was also noticed due to alloying. SEM study of wear surface and wear debris was conducted to analyse the mode of wear and wear mechanism.

L. Lasa and J. M. Rodriguez-Ibabe [27] studied the effect of composition and processing route on the wear behaviour of Al–Si alloys. The wear behaviour of five Al–Si alloys, with Si contents between 12% and 16% and different Cu and Ni additions, has been studied using pin-on-disc tests. The importance of alloying elements and alloy processing has been proven. New thixoformed microstructures showed better wear resistance than alloys produced in metallic moulds.

The alloy composition is given in the table 4.1. Alloys H3, H4 and H6 were cast in permanent metallic moulds by Hydro Aluminium. Alloys H3 and H4 were Na and Sr modified; alloy H6 was not. The alloys were tested both as-cast and after T6 heat treatment. The parameters developed for the heat treatments were: solutioning at 500°C for 5 h in a salt bath (except alloy thixo477 that was solution heat treated for 3 h), water quenching at room temperature and artificial ageing in an oil bath at 180 °C for 4 h.

Two different test conditions were used (A and B). The load applied was 46.51 N and the distance 2000 m in both of them; the speed of the disc varied between 0.089 and 0.356 m/s for condition A and B, respectively.

Table 4.1:Chemical composition (wt%) and hardness of the alloys.

Alloy	Chemical composition						Hardness (HRB)	
	Si	Mg	Cu	Ni	Fe	Ti	As-cast	After T6
H3	12.85	1.30	1.13	0.00	0.11	0.11	45	77
H4	12.29	1.30	4.40	0.00	0.12	0.11	58	86
H6	15.90	1.20	4.71	0.00	0.12	0.11	67	91
477	15.30	0.58	4.38	<0.42	0.21	0.16	68	89
501	15.70	0.54	4.56	4.10	–	0.17	77	87

Alloys H3 and H4 have both nearly the eutectic composition. The microstructure consists mainly of the eutectic aluminium silicon phase with very few primary silicon particles that are evenly distributed in the matrix. Alloy H6 was not modified and as a

consequence, the microstructure is completely different. This alloy consists of a very fine eutectic aluminium–silicon phase with a few clusters of massive primary silicon particles.

Thixoformed alloys thixo477 and thixo501 exhibit a very homogeneous microstructure; they contain an aluminium globules, a high fraction of primary silicon particles and a fairly small amount of eutectic aluminium–silicon and intermetallic particles surrounding the aluminium globules and forming small pockets. The microstructures of the alloys are shown in Figure 4.18. The wear rate of the alloys at both testing conditions is shown in Figure 4.19. The overall response of these alloys was very different at the two conditions considered.

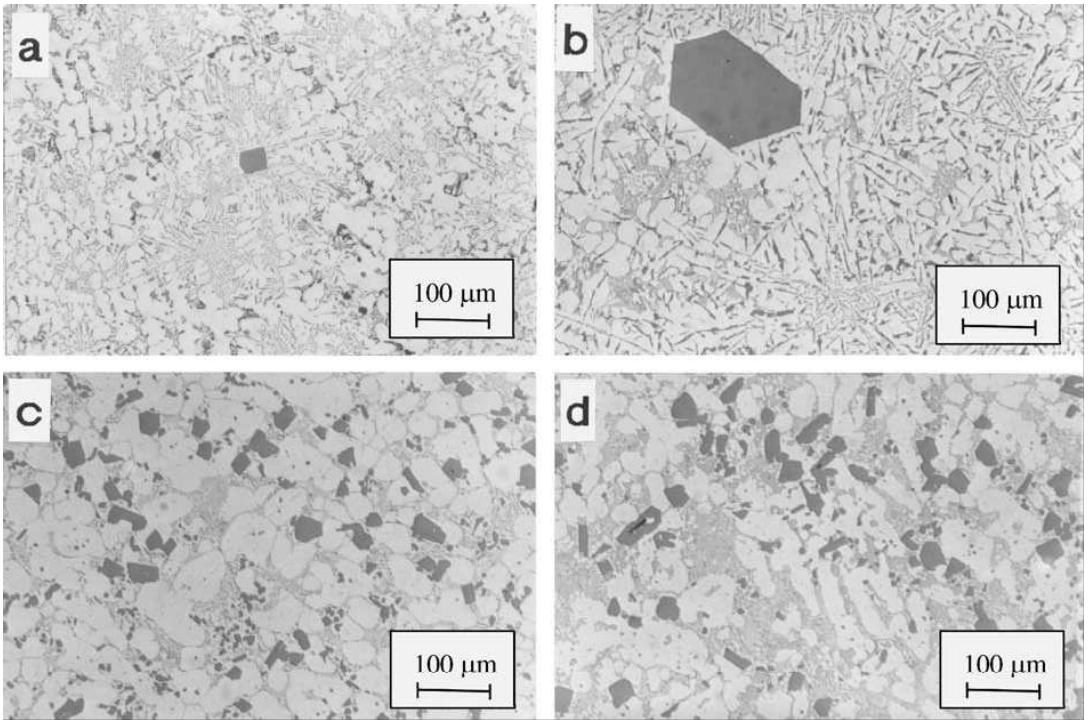

Figure 4.18. Microstructures of the alloys: (a) H3; (b) H6; (c) thixo477; (d) thixo501. Notice a aluminium phase in white, eutectic and primary silicon partic--les in dark grey and intermetallics in light grey.

Under condition A, the effect of alloy composition was very marked. Alloys H3 and H4 have similar composition and microstructures but the additional Cu content of alloy H4 makes it more resistant to wear. Comparing the response of alloys H4 and H6, the beneficial effect of the higher silicon content is clear too. Nickel does not seem to have any remarkable influence upon wear. However, it should be noted that alloy thixo501 with 4.1% Ni content performed slightly better than alloy thixo477 with less than 0.42% of Ni. The fine homogeneous microstructure of both thixoformed alloys greatly improved the resistance to wear. The smaller spacing of the primary silicon particles in these alloys could be responsible for this improvement The T6 heat treatment did lower the coefficient of wear of alloys H3 and H4, but no significant change was apparent in the rest of the alloys.

The higher coefficient of wear observed in alloys H3 and H4 was due to the transition in wear mechanism that took place during the tests. This transition was less pronounced for alloy H6 and non-existent for both thixoformed alloys. The heat treatment improved the wear resistance of alloys H3 and H4 by means of delaying the transition as can be seen in Figure 4.20 where the loss of pin height as a function of distance is plotted.

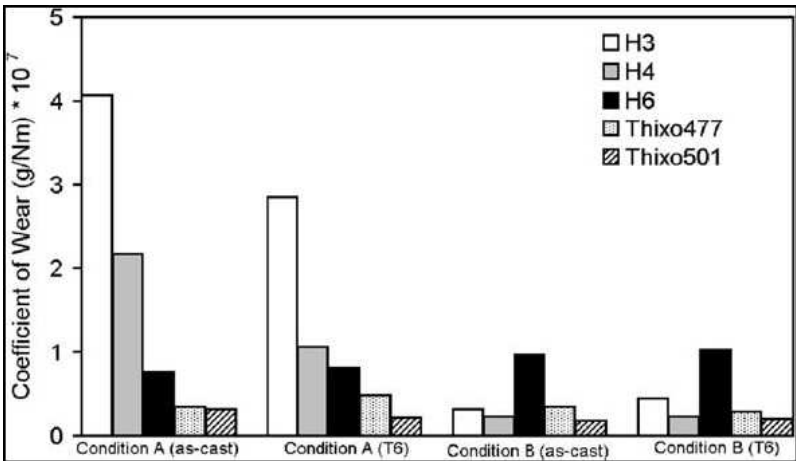

Figure 4.19: Coefficient of wear of the alloys as a function of testing condition.

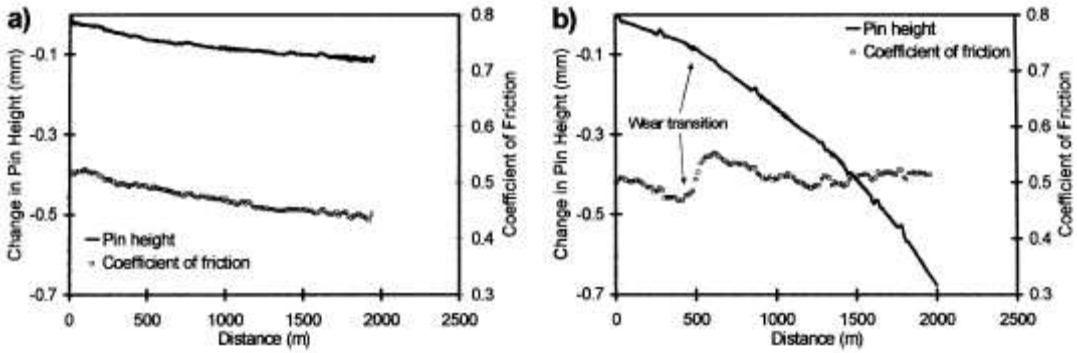

Figure 4.20: Change in coefficient of friction with transition in wear: (a) alloy thixo501; (b) alloy H4.

Under condition B, the higher disc speed reduced the experiment time by four. The disc surface did not suffer so much contamination from the wear debris, the protective oxide layer remained stable on the pin surface and consequently all the alloys, with the exception of alloy H6, suffered less wear. In alloy H6 the higher disc speed of condition B provoked the rupture of some of the big silicon particles, giving rise to deep wear groves and, in consequence, increasing the coefficient of wear.

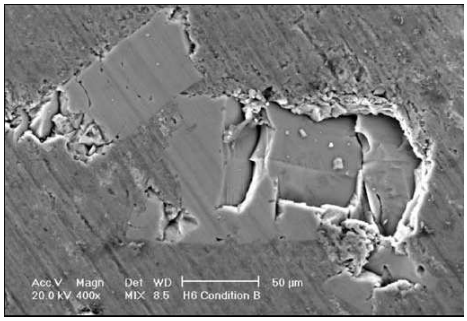

Figure 4.21: Pull-out of the silicon particles in alloy H6 during test under condition B.

Under constant load and test distance conditions, the coefficient of wear of the alloys studied is highly dependent on the disc speed. At the faster disc speed of 0.356 m/s, the mechanism of wear was found to be of oxidative nature and all the alloys suffered low to moderate wear. At the slower speed of 0.089 m/s, lower Cu and Si contents led to accelerated transition to adhesive wear and consequently the wear rate increased

dramatically (Figure 4.21). The fine homogeneous microstructure of both thixoformed alloys improved the wear resistance by inhibiting completely the transition to adhesive wear.

The heat treatment improved the wear of the low silicon content alloys under low speed but the influence upon the rest of the alloys was non-existent.

CHAPTER – 5

EXPERIMENTAL WORK

In this chapter all the details about the preparation and characterization of samples has been described. In the present work, the casting technique has been utilized to prepare the samples of aluminium alloys. The experiment technique involves following steps:

- Casting
- Preparation of samples
- Characterization & Testing

The alloy composition that is selected for present study is:

SET - I

Elements	Al (wt%)	Si (wt%)	Pb (wt%)	Sn (wt%)	Cd (wt%)	Bi (wt%)	Alloy comp.(wt%)
Sample-1	87.4	12.6	--	--	--	--	Al-12.6%Si
Sample-2	82.9	12.6	4.5	--	--	--	Al-13.19%Si
Sample-3	82.9	12.6	--	4.5	--	--	Al-13.19%Si
Sample-4	82.9	12.6	--	--	4.5	--	Al-13.19%Si
Sample-5	82.9	12.6	--	--	--	4.5	Al-13.19%Si

SET – II

Elements	Al (wt%)	Si (wt%)	Cu (wt%)	Pb (wt%)	Sn (wt%)	Cd (wt%)	Bi (wt%)	Alloy comp.(wt%)
Sample-1	82.9	12.6	4.5	--	--	--	--	Al-13.19%Si
Sample-2	78.4	12.6	4.5	4.5	--	--	--	Al-13.84%Si
Sample-3	78.4	12.6	4.5	--	4.5	--	--	Al-13.84%Si
Sample-4	78.4	12.6	4.5	--	--	4.5	--	Al-13.84%Si
Sample-5	78.4	12.6	4.5	--	--	--	4.5	Al-13.84%Si

Purity level of metals:

- Aluminium – 99.99%
- Silicon – 99.9%
- Copper – 99.5%
- Lead – 99.5%
- Tin – 99.5%
- Cadmium – 99.5%
- Bismuth – 99.5%

5.1 Casting

Equivalent quantities of the various metal granulars were taken by weight. For making each 100gm batch, the weighing was done in a very accurate weighing balance (Sigma).

For e.g. for **Set –I:**

Sample I (Al- 12.6%Si) the quantities of the metals taken as:

Al = 87.4gm

Si = 12.6gm

Similarly,

Set-II:

Sample I (Al- 12.6%Si-4.5%Cu)

Al = 82.9gm

Si = 12.6gm

Cu = 4.5gm

For each sample after weighing metal granulars, they are put into the fire-clay crucible. Then the crucible with metal charge is placed into the Indfur electric furnace (muffle furnace) which is heated upto 750°C and metal is allowed to melt. Stirring is done while melting for complete mixing of charge. When all the granulars melt and mixed completely, the molten metal is removed from the furnace and poured into an iron mould. After allowing the metal to cool and solidify in the shape of the mould, the casted samples are taken out of mould.

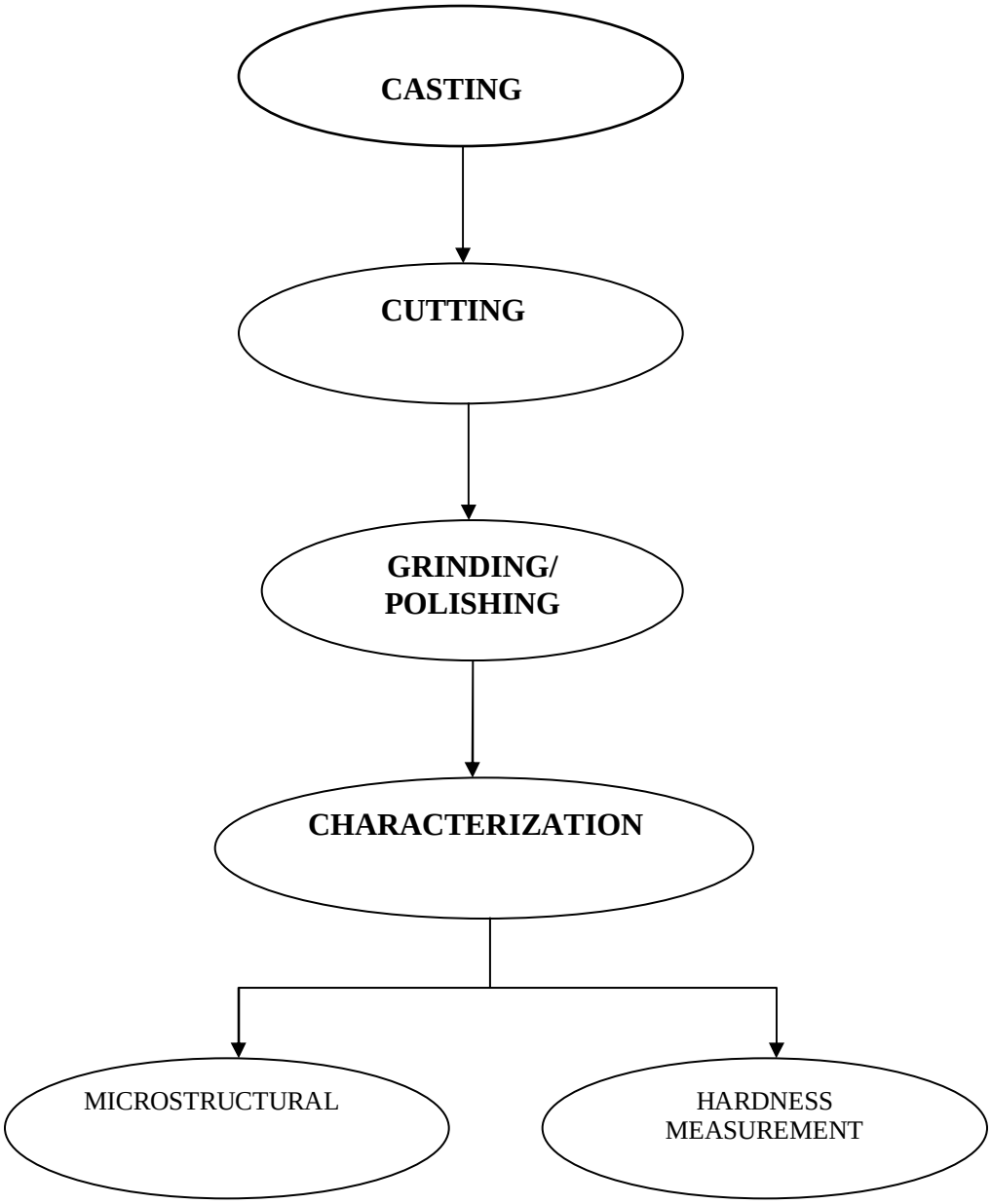

Figure 5.1: Flow chart showing the whole experimental work

5.2 Sample preparation

5.2.1 Cutting

The cast samples are cut in the transverse direction with the help of hexa in the four equal parts. The one of the piece of the cut sample is used for sample preparation.

5.2.2 Grinding/polishing

The cut samples prepared above had an uneven surface. So the cut samples were then taken for the grinding/polishing operation. The sample was first held over a grinding machine with a moving belt to obtain a smooth surface. The grinding is done in such a way so that all the scratches are in the same direction and the grinded surface becomes flat. After this the samples are polished properly using different grits of emery paper. Because the samples being aluminium alloy, aluminium being soft, it is rubbed over the 400 and 600 grit emry paper for a small time. Then it was rubbed over an emry paper of 800 grit and then over a very fine emry paper of 1000 grit for a considerable time in order to get a smooth and clear surface of the sample.

The sample was then polished on a fine polishing machine using an alumina polish. This was done to get a well polished and a smooth surface required for the further characterization of the samples.

Similarly all the samples were polished for a considerable time, over and over again until a very fine and smooth surface was obtained.

5.3 Characterization

- Microstructural Characterization
- Hardness Measurement

5.3.1 Microstructural characterization

The well-polished samples were then observed under an optical microscope. Micrographs were taken with the help of CCD camera attached to the optical microscope and are further viewed on computer with optical image analyzer software at magnification of 200X and 400X for all the different samples.

5.3.2 Hardness measurement

Hardness of all the samples is measured before and after the aging treatment. For aging treatment the muffle furnace is first preheated to 150°C temperature after that the samples are put inside the muffle furnace (Navyug India) for the 2 hr. duration. After 2 hrs the samples are quenched in distilled water and change in hardness after quenching is measured. Now the samples are allowed to age hardened at room temperature and hardness of each samples are measured with time intervals. The hardness of each sample has been measured on Mitutoyo hardness testing machine which comprises of Vickers hardness number.

5.3.2.1 Vickers Hardness Test

It is the standard method for measuring the hardness of metals, particularly those with extremely hard surfaces: the surface is subjected to a standard pressure for a standard length of time by means of a pyramid-shaped diamond. The diagonal of the resulting indention is measured under a microscope and the Vickers Hardness value is calculated by putting the valued in the formula. The Vickers Diamond Pyramid harness number is the applied load (kgf) divided by the surface area of the indentation (mm^2).

Microhardness test was done for the various samples using the Vicker's Hardness machine. The readings of the indent obtained were taken and the corresponding

VHN (H_V) was obtained. Three to five readings were obtained for each sample at different phases, while observing from the microscope in the Vicker's Hardness machine. The formula used is:

$$H_V=1.854\ F/\ d^2$$

Where:

F=Load in kgf

d = Arithmetic mean of the two diagonals, d1 and d2 in mm

H_V = Vickers hardness

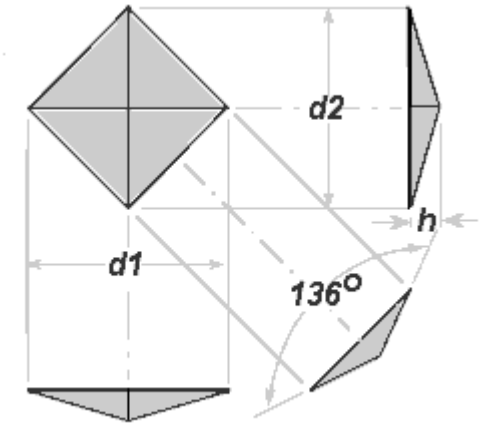

Figure 5.2: Vickers Pyramid Diamond Indenter Indentation

A constant load of 100 gm was applied for 15 seconds on different samples. The results obtained were then tabulated and a graph prepared by taking the time at which the sample's hardness was measured against the H_V.

CHAPTER-6

RESULTS AND DISCUSSIONS

6.1 Microhardness test

Microhardness of each sample was measured in the Al-Si rich phase (white). The reason for this was to see the feasibility of providing hard matrix with proper distribution of the softer phase into it. Hardness measurement was done to see the feasibility of this material as a bearing material as hardness and wear characteristics are related to each other upto a greater extent. A variation in hardness was observed for the samples of Al-Si-Cu in the entire range of time intervals.

The readings obtained for various samples by using the Vicker's Hardness testing machine are tabulated below:

Table 6.1 change in H_V w.r.t aging time for the samples:

SET-I SAMPLE-1, Al-12.6%Si

SET-II SAMPLE-1, Al -12.6%Si -4.5%Cu

Time(hr.)	Set-I, Sample1		Set II, Sample 1	
	Corresponding H_V	Average H_V	Corresponding H_V	Average H_V
0	68.565	68.8	94.68	105.549
	67.5867		100.852	
	70.243		121.1156	
1	69.56,66.92	68.34	97.416,95.76	108.998
	68.564		102.0424,108.96	
	64.47		117.34,107.65	
3	65.3836,64.172	67.679	108.958,120.144	109.306
	66.946,66		99.638,114.44	
	67.9104,75.664		100.2704,112.336	
4	66.3144	65.729	100.27,98.54	110.021
	67.5864		118.827	
	63.286		110.967	
5	77.2176		100.27	107.99

	66.3144	69.234	106.364	
	64.1728		117.36	
6	74.907	68.439	115.875	113.652
	61.348		118.0784	
	68.564		107.004	
7	67.5864	68.372	103.36	111.391
	66.946		115.875	
	70.5864		114.44	
18	66.628	70.436	110.92	112.36
	72.6934		113.3	
	71.984		112.86	
22	68.8956	67.74	113.0	113.0
	64.472		113.0	
	69.56		113.0	
26	62.12	67.08	130.964	119.028
	69.228		110.9668	
	69.9028		115.154	
30	70.56	70.132	138.215	127.016
	69.9004		128.3932	
	75.664		114.44	
42	76.436	75.743	130.099	130.099
	75.28		130.99	
	75.28		130.99	
46	73.422	72.001	121.893	130.599
	72.34		134.48	
	70.2432		135.424	
51	70.9	72.43	135.42	131.016
	77.216		129.24	
	69.2		128.39	
55	69.23	71.19	131.52	132.64
	67.91		134.72	
	76.4358		131.68	
66	75.664	74.174	133.6156	133.125
	74.16		142.0672	
	72.6984		126.72,130.1	

70	72.69	73.16	135.427	141.46
	73.424		135.427	
	73.4		153.5324	
118	73.06	72.346	137.276	135.46
	71.28		137.276	
	72.6987		131.84	
126	66.002	74.1562	125.08	138.813
	77.2178		150.271	
	80.468		141.089	
132	74.16	71.065	141.089	135.234
	70.5865		130.099	
	68.2366		134.516	
140	76.04	69.216	119.583	129.85
	62.7		136.347	
	74.91		133.62	
155	71.28	73.9	126.72	128.42
	73.9		138.21	
	74.907		120.34	
162	76.825	73.029	130.1,118.08	125.305
	72.6988		110.97	
	69.595		142.07	
179	66.00	69.35	45.875	120.781
	74.16		118.079	
	67.91		128.39	
187	74.91	71.14	117.337	122.23
	70.59		125.396	
	67.91		123.47	
199	78.81	72.99	123.47	120.91
	71.28		116.60	
	68.89		122.678	
210	74.532	71.564	116.603	119.975
	69.229		126.72	
	70.932		116.603	

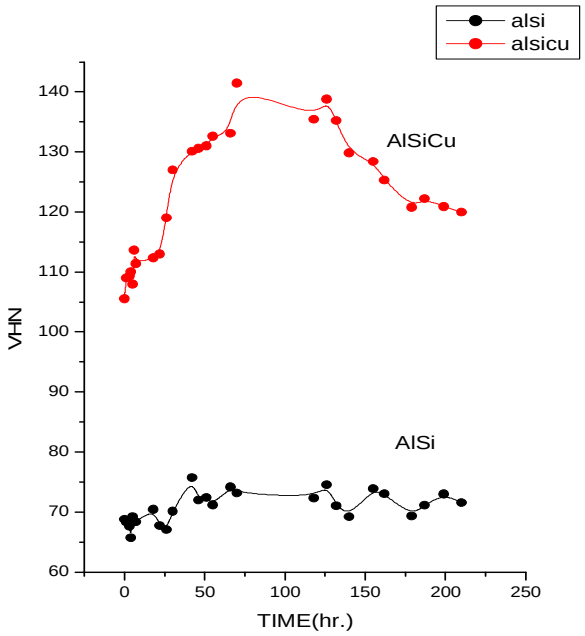

Figure6.1:Change in microhardness w.r.t. aging time for sample-1 of set-I and set-II

Figure 6.1 shows the natural aging plots for the Al-Si and Al-Si-Cu alloys. From the figure it is completely evident that the overall hardness provided by Al-Si-Cu is much higher than the Al-Si alloy. This is due to the strenghthening phenomenon provided by the addition of Cu in the Al-Si-Cu alloy. Moreover the composite Al-Si-Cu shows the increase in the hardness and attains peak hardness (141.46 H_V) at 70 hr. but the plotted line of Al-Si do not show such increase in hardness with aging time. This can be explained on the basis of precipitation hardening phenomenon shown by Cu present in Al-Si-Cu alloy. According to this phenonmenon a variety of different precipitate structures is formed below the solvus line. As In alloys of Al-Cu system, a succession of precipitates is developed from a rapidly cooled supersaturated solid solution (SSS). These precipitates develop sequentially either with increasing temperature or with increasing time at temperatures between room temperature and the solvus. The several stages are identified by following notation:

$$SSS \longrightarrow \text{GP zones} \longrightarrow \theta' \longrightarrow \theta'' \longrightarrow \theta(Al_2Cu)$$

These GP zones are coherently embedded in the matrix, which provide the increase in hardness phenomenon and the decrease after the peak is due to the growth of incoherent precipitates during overaging.

Table 6.2 Change in H_V w.r.t aging time for the samples :

SET-I SAMPLE-2, Al -12.6%Si -4.5%Pb

SET-II SAMPLE-2, Al -12.6%Si -4.5%Cu -4.5%Pb

Time (hr)	Set-I, Sample 2		Set-II, Sample 2	
	Corresponding H_V	Average H_V	Corresponding H_V	Average H_V
0	69.56	64.93	119.5829	97.174
	62.99		86.20	
	62.99		85.74	
	64.173			
1	65.079,68.896	65.18	103.8616	101.496
	62.996		93.624	
	59.64,63.58		107.004	
3	63.58,68.896	65.244	103.254	103.254
	62.996,66.628		95.764	
	66.946,62.4188		100.268	
4	63.58	66.915	98.544	101.533
	69.90		95.7644	
	67.2652		110.29148	
5	59.1196	64.3	100.268,92.58	104.101
	63.876		113.0,110.28	
	69.903		107.64,100.84	
6	69.23	64.085	109.622,99.1144	106.452
	64.17		99.1144	
	58.86		115.875	
7	65.38	69.49	105.728	104.345
	79.224		107.648	
	63.874		99.688	
18	65.69	66.13	114.44	110.857
	67.91		105.102	
	64.79		113.0312	
22	61.85	63.5	101.444	111.661
	64.77		121.892	
	63.88		111.648	
26	64.774	64.774	126.76	118.372
	64.774		110.28	
	64.774		118.076	

30	74.53	75.84	125.896	117.78
	65.38		121.08	
	87.61		106.364	
42	78.41	74.02		
	73.06			
	70.59			
46	74.532	72.28	117.7336	122.034
	79.64		115.152	
	73.42		133.6156	
51	70.934	72.281	129.24	126.476
	70.24348		126.72	
	75.6656		123.47	
55	74.90	73.19	144.44	127.349
	73.06		123.417	
	71.63		120.344,120.334	
66	73.42	75.43	113.276	128.539
	75.66		139.1628	
	77.22		121.1158	
74	70.59	70.36	140.12	140.308
	69.90		126.72	
	70.59		158.048,130.347	
118	72.70	72.36	137.27	135.58
	74.16		128.39	
	72.34		141.08	
	70.24			
126	63.31	70.09	126.72	135.135
	71.98		121.893	
	71.98		159.21,132.72	
132	68.24	69.13	121.1158	122.759
	74.16		132.723	
	65.08		114.44	
140	70.24	69.29	123.47	123.44
	71.63		141.1	
	66.0		119.58,109.62	
155	66.95	68.4	133.61	131.75
	71.63		142.067	
	66.63		119.58	
162	65.69	71.25	122.67	126.53
	69.23		131.84	
	78.82		125.08	
179	72.69	71.81	121.89	123.08
	70.93		124.27	
187	67.27	68.92	102.64	121.598
	70.59		119.58	

			135.427	
199	79.184	73.26	116.603	121.66
	74.532		126.72	

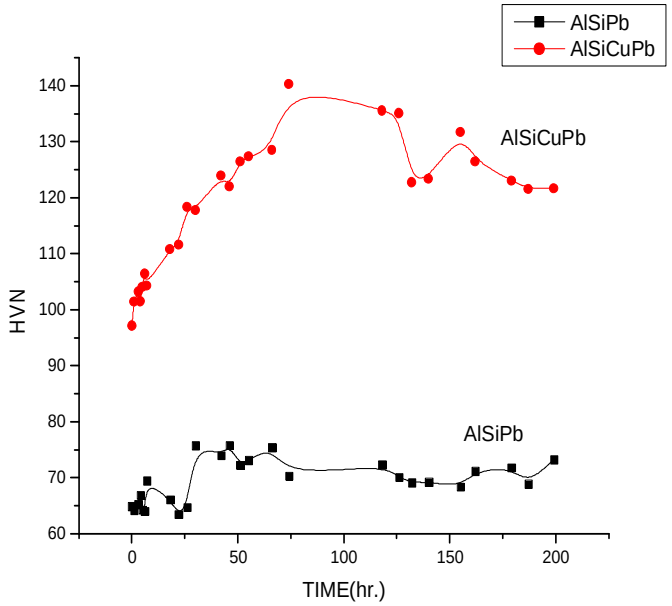

Figure6.2: Change in microhardness w.r.t. aging time for sample2 of set-I and set-II

A similar characteristic in the behavior of hardness was also observed for the samples containing Pb (Figure 6.2). Hardness increasing trend is same as in the Al-Si-Cu alloy and peak got maxima at 74 hr (140.3 H_V). However lead is added in these samples to provide lubrication property. Thus the sample provides the lubrication property with the same hardness as Al-Si-Cu alloy.

Table 6.3: Change in H_V w.r.t aging time for the samples:

SET-I SAMPLE-3, Al -12.6%Si -4.5%Sn

SET-II SAMPLE-3, Al -12.6%Si -4.5%Cu -4.5%Sn

Time (hr)	Set-I, Sample 3		Set-II, Sample 3	
	Corresponding H_V	Average H_V	Corresponding H_V	Average H_V
0	61.848	61.848	84.3776	89.108
	61.848		92.5812	
	61.848		90.5464	
1	58.3356	65.266	89.52	90.208
	68.236		91.552	
	69.228		89.554	
2	62.992	63.485	94.684	92.322
	64.472		87.6	
	62.992		94.684	
3	61.288	63.347	97.38	91.51
	60.1896		89.552	
	68.564		87.6	
4	67.744	65.789	93.624	96.166
	66.92		99.112	
	62.704		95.764	
5	64.794	65.598	103.248	100.43
	66.0		94.684	
	66.0		103.86	
6	75.664	71.597	101.44	101.884
	69.9		99.112	
	69.228		105.1	
7	78.412	73.960	95.2224	104.386
	68.5652		99.1144	
	74.904		118.824	
9	70.584	69.692	104.232	104.232
	70.584		106.3644	
	67.9104		111.6488	
21	78.816	70.481	100.27	103.61
	66.6292		110.29	
	66.0		100.27	
25	67.908	70.99	107.648	101.46
	73.7904		102.0424	
	71.28		94.684	
29	66.946	72.921	117.336	108.986
	67.9104		97.976	
	83.0432		111.648	
	73.7888			

33	70.5864	70.248	107.00	105.898
	70.932		103.25	
	69.228		105.10	
44	74.532	76.459	110.291	105.116
	76.4356		108.958	
	78.412		99.1145	
52	69.229	72.54	102.644	111.488
	70.5865		105.102	
	80.46875		126.72	
	69.9029			
96	73.7905	74.264	129.24	117.3
	79.6370		103.86	
	72.6987		113.827	
	70.932			
108	69.90	69.175	110.967	116.18
	71.98		118.79	
	67.586			
	67.586			
124	73.79	68.988	110.967	112.231
	66.629		107.00	
	66.946		118.786	
132	66.0	66.315	110.967	112.6
	66.315		110.967	
	66.65		115.875	
148	67.91	65.288	100.36	107.67
	67.265		100.36	
	63.28		110.29	
	62.70			
154	74.16	71.329	105.10	104.27
	68.896		104.48	
	70.932		103.25	
171	68.565	67.49	105.73	107.66
	66.0		107.64	
	67.91		109.62	
179	66.63	67.27	106.3	105.28
	67.91		106.3	
	62.42		103.25	
191	70.24	68.4345		
	66.629			

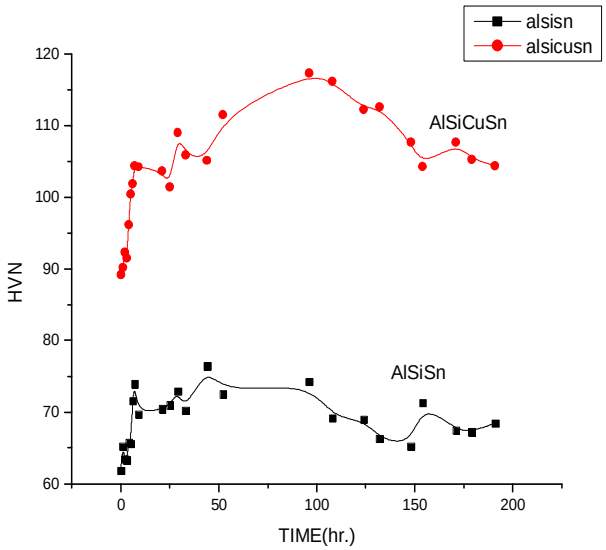

Figure6.3: Change in microhardness w.r.t. aging time for sample3 of set-I and set-II.

Here in figure 6.3 the trend is also same in increasing hardness due to precipitate formation during aging of the Al-Si-Cu-Sn alloy. In this case peak is attained at 96hr. and the hardness value is 117.3 H_V, which is smaller than previous Al-Si-Cu and Al-Si-Cu-Pb. Sn is added to provide dimensional tolerances and good embeddability to the alloy. However the Al-Si-Sn alloy do not show any much increase in the hardness phenomenon.

Table 6.4: Change in H_V w.r.t aging time for the samples :

SET-I SAMPLE-4, Al -12.6%Si -4.5%Cd

SET-II SAMPLE-4, Al -12.6%Si -4.5%Cu -4.5%Cd

Time (hr)	Set-II, Sample 4		Set-I, Sample 4	
	Corresponding H_V	Average H_V	Corresponding H_V	Average H_V
0	118.08	114.96	89.06	86.24
	111.65		84.378	
	115.15		85.29	
2	118.83	119.59	85.285	84.46
	119.58		87.62	
	120.35		80.469	
3.5	113.03	115.15	87.144	87.144
	117.34		87.144	

	115.15		87.144	
6	121.89	119.36	86.673	88.201
	119.58		84.83	
	116.60		93.1	
8	114.44	115.398	83.93	85.3
	116.6		86.67	
	115.154			
17	113.03	115.97	92.07	85.85
	118.83		86.67	
	113.73		78.82	
23	120.35	127.753	88.58	85.95
	134.52		82.61	
	128.39		86.67	
26	130.1	120.397	87.62	86.52
	121.12		86.21	
	113.03		85.74	
	117.37			
28	126.72	119.8	86.67	83.59
	112.34		84.14	
	124.27		80.89	
	115.86		79.64	
30	115.88	115.5	90.05	88.602
	110.29		89.55	
	120.35		86.21	
71	124.24	115.91	84.83	87.174
	115.154		89.55	
	108.3		87.14	
94	112.34	112.6	86.207	87.15
	115.15		87.14	
	110.29		88.096	
100.5	109.62	113.31	81.31	82.32
	115.875		82.61	
	114.44		83.04	
102.5	107	113.36	76.44	83.28
	115.88		84.83	
	118.03		88.58	
117	111.65	113.98	89.064	87.16
	115.88		85.74	
	114.44		86.67	
121	115.15	117.37	80.89	81.779
	119.58		84.74	
			86.67	
124	113.73	113.38	78.41	82.095
	113.03		83.04	
			84.83	

145.5	114.44	113.98	81.74	83.06
	111.65		82.17	
	115.88		85.28	
145.5	118.079	114.02	88.598	86.758
	109.62		82.61	
	110.29		89.07	
	118.08			
148	113.032	113.24	83.285	84.581
	106.36		87.14	
	120.35		81.31	

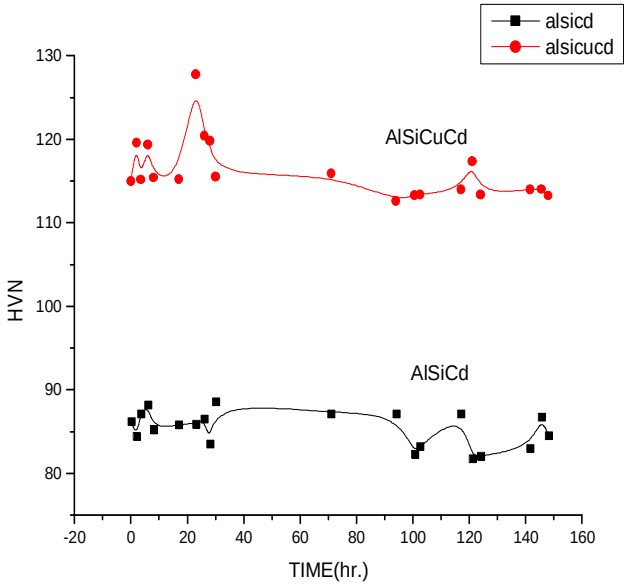

Figure6.4: Change in microhardness w.r.t. aging time for sample4 of set-I and set-II

Here Cd is added to the Al-Si and Al-Si-Cu alloys. Due to presence of Cu in the alloy hardness peak is achieved at 23 hr. of aging corresponding 127.7 H_V. But the similar results in the case Al-Si-Cd that it does not show any increasing hardness trend. However the overall hardness of Al-Si alloy is increased on addition of Cd than that of Al-Si. Cd metal being soft is incorporated to Al-Si alloy to provide better surface and mechanical properties.

Table 6.2 Change in H_V w.r.t aging time for the samples:

SET-I SAMPLE-5, Al -12.6%Si -4.5%Bi

SET-II SAMPLE-5, Al -12.6%Si -4.5%Cu -4.5%Bi

Time (hr)	Set-I, Sample 5		Set-II, Sample 5	
	Corresponding H_V	Average H_V	Corresponding H_V	Average H_V
0	85.749	82.4	147.11	142.11
	81.74		145.06	
	80.051		133.62	
2	76.05	78.29	142.07	147.9
	74.91		149.2	
	83.93		152.43	
3.5	76.82	78.1	139.16	137.90
	81.74		137.28	
	75.67		137.28	
6	73.06	77.09	143.055	138.16
	82.17		134.516	
	76.05			
8	82.17	85.33	141.08	139.65
	87.62		138.22	
	86.2			
17	82.17	82.92	156.9	152.53
	85.28		148.55	
	81.31			
23	78.61	82.03	153.53	145.87
	85.74		138.21	
	81.74			
26	80.47	82.48	152.43	148.29
	84.38		151.35	
	82.01		141.1	
28	78.01	80.16	138.21	139.51
	76.74		150.27	
	85.28		130.1	
	80.88			
30	79.64	78.03	143.06	132.43
	72.7		122.68	
	81.74		131.84	
71	76.05	75.11	140.1	134.15
	75.66		134.52	
	73.06		133.60	
			128.39	
97.5	78.01	76.45	138.2	150.9

	76.05		154.56	
	75.29		161.56	
			149.21	
100	75.67	73.69	134.52	132.57
	73.79		128.39	
	71.63		130.1	
			137.27	
102.5	77.67	75.67	136.35	133.84
	73.6		121.12	
			114.05	
117.5	74.16	77.55	154.64	145.23
	77.61		131.84	
	80.89		149.21	
121	74.16	71.91	131.84	140.63
	69.23		135.43	
	72.34		154.64	
124	72.69	72.95	146.08	145.39
	71.98		154.64	
	74.16		135.47	
143	74.16	75.4	137.27	130.2
	80.05		122.68	
	71.98		130.1	

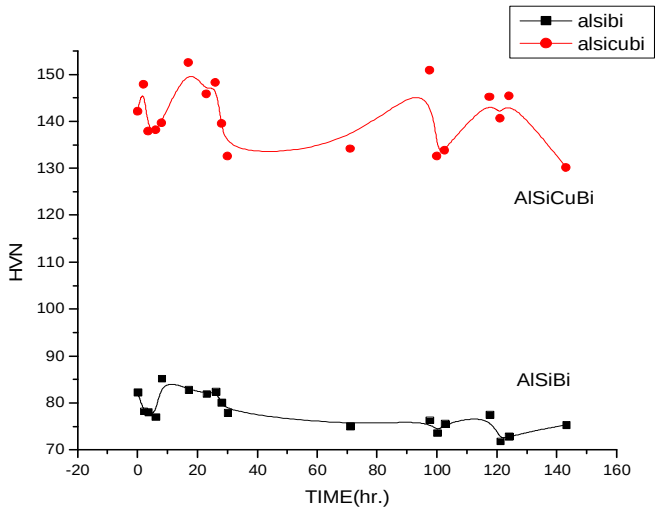

Figure6.5: Change in microhardness w.r.t. aging time for sample5 of set-I and set-II

On the addition of Bi to the Al-Si-Cu alloy however do not show any increase in the hardness behaviour (figure 6.5) as shown in the previous results but due to presence of Cu and Bi the overall hardness of Al-Si alloy is increased.

6.2 Microstructural Analysis

Microstructural features are the key features that provide the backbone for the wear characteristics of all the materials. A detailed study of the microstructural features of all the samples was carried out for the samples.

6.2.1 Optical micrographs of before aging treatment

Optical micrographs provide the structural features of the sample being studied. The samples are prepared with different alloying elements via casting route. The micrographs are being taken after well polishing the sample at higher magnification.

6.2.1.1 Micrographs of SET-I

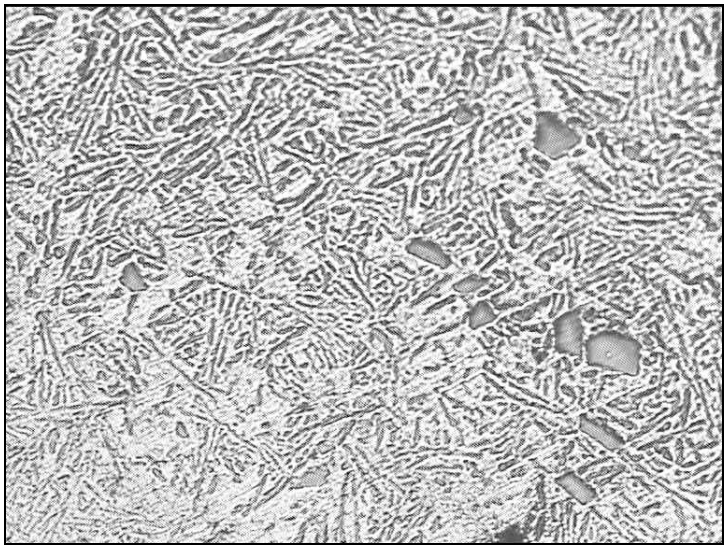

Figure 6.6: Micrograph of Sample-1 Al-12.6%Si at 200X.

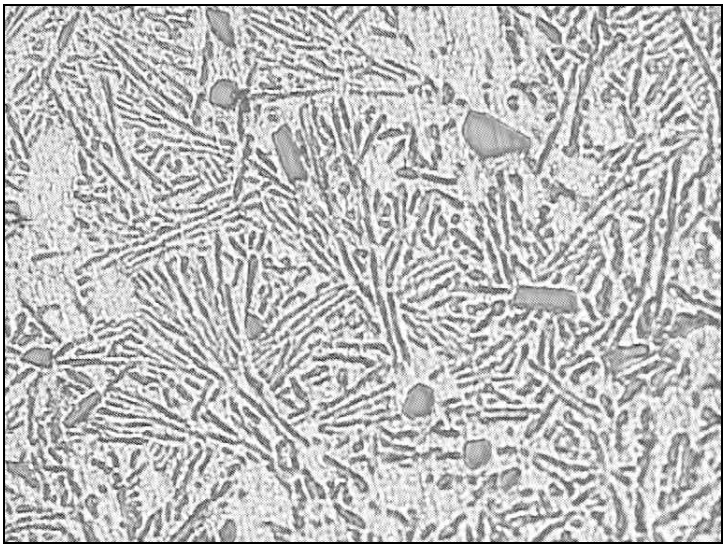

Figure 6.7: Micrograph of Sample-2 Al -12.6%Si -4.5%Pb at 200X.

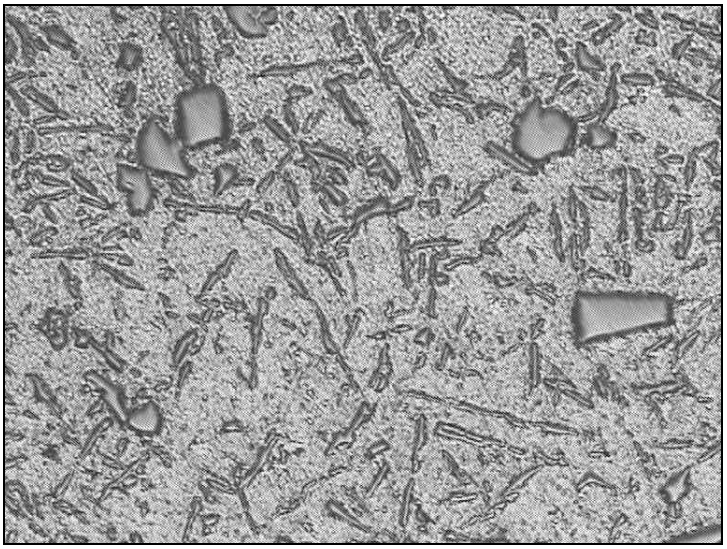

Figure 6.8: Micrograph of Sample-3 Al -12.6%Si -4.5%Sn at 200X.

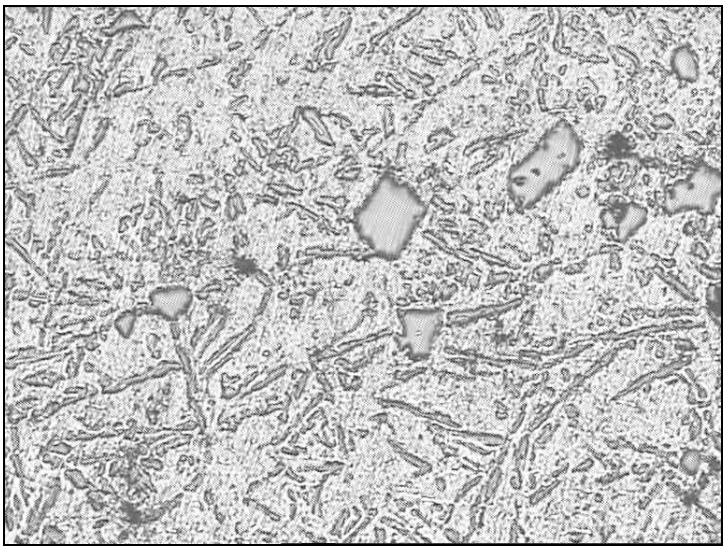

Figure 6.9: Micrograph of Sample-4 Al -12.6%Si -4.5%Cd at 200X.

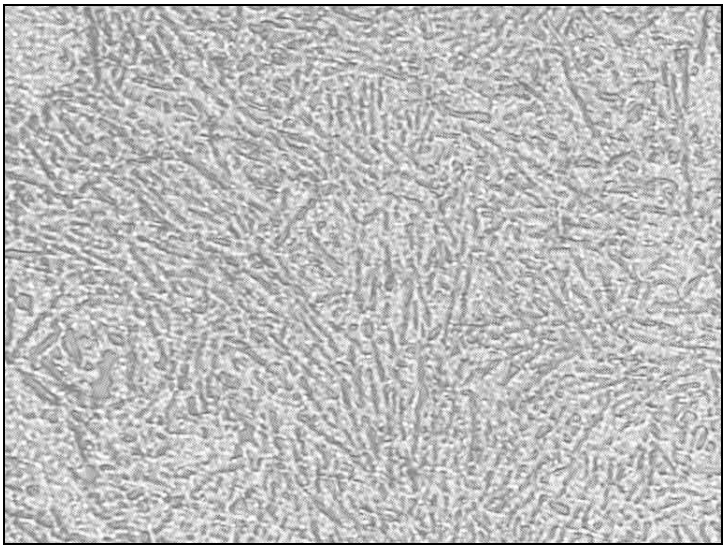

Figure 6.10: Micrograph of Sample-5 Al -12.6%Si -4.5%Bi at 400X.

The micrographs of samples prepared for set-I are shown in figure6.6 to figure6.10. The micrographs indicate lots of variation in structural features. For sample 1, Al-12.6% Si the structure is eutectic in nature. Therefore typical features observed in sample 1 is needle like structure of Si uniformly distributed in the white matrix of Al as shown in figure 6.6 taken at magnification 200X. However, primary silicon can be seen as embedded particle inside the matrix.

On addition of Pb we can see that the structural features are similar to that of eutectic type of structure means the addition of lead does not modify the structure. Also no separate morphological feature is visible for lead alloying. But on critical analysis it can be seen that the growth the secondary silicon phase has occurred from the interface where the primary silicon exists. The overall features appear to be rosette type of structure comprising of Si needles as shown in figure 6.7.

In case of Sn and Cd addition the structural features of silicon appears to be blunt and twisted type visible in figure 6.8 and figure 6.9. The structural variation exists in the form of transition of the silicon phase which tries to acquire the spherical shape by getting the Si needle stretched. Though the structure looks to be uniform but here also the presence of primary silicon phase exists. The amount of primary phase in case of Cd is somewhat higher than Sn. In case of Cd similar results has been observed by W.Y. Yoon [28] on addition of 2% Gd in Al-14%Si alloy.

In case of Bi, it modifies the structural features of the alloy as shown in micrograph figure 6.10 taken at higher magnification 400X. Bi leads the structural feature to the columnisal development of the eutectic phase and very fine needle like structure with complete mixing of Bi in matrix is observed. It forms complete eutectic type structure.

6.2.1.2 Micrographs of SET-II

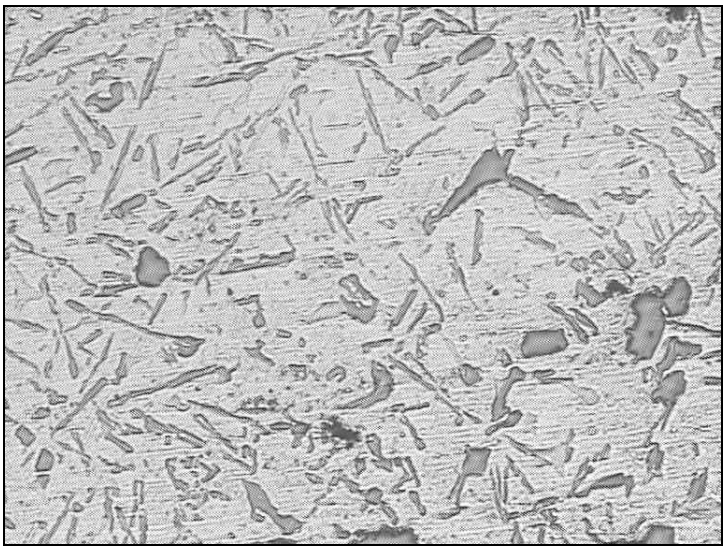

Figure 6.11: Micrograph of Sample-1 Al -12.6%Si -4.5%Cu at 200X.

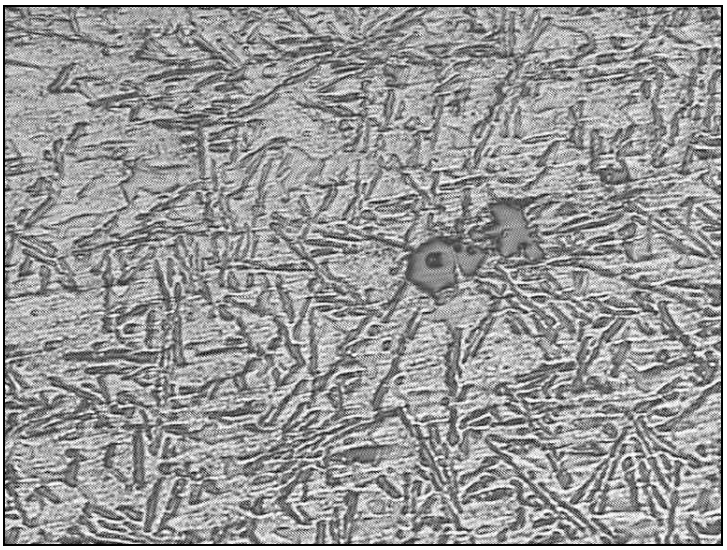

Figure 6.12: Micrograph of Sample-2, Al -12.6%Si -4.5%Cu -4.5%Pb at 200X.

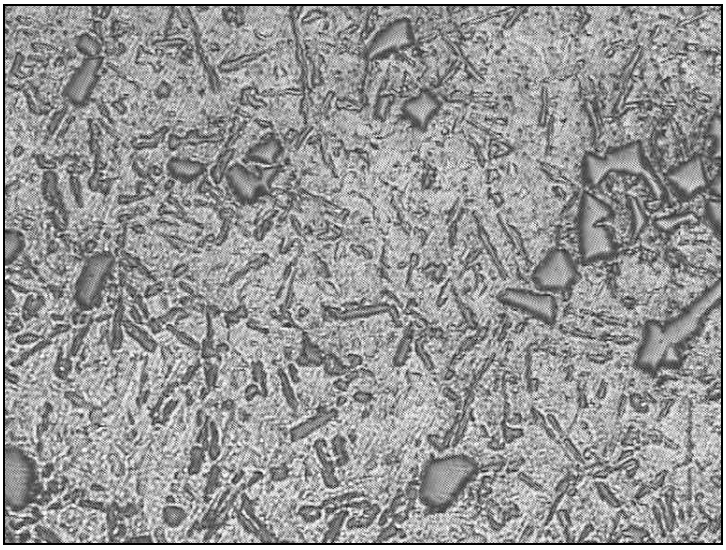

Figure 6.13: Micrograph of Sample-3, Al -12.6%Si -4.5%Cu -4.5%Sn at 200X.

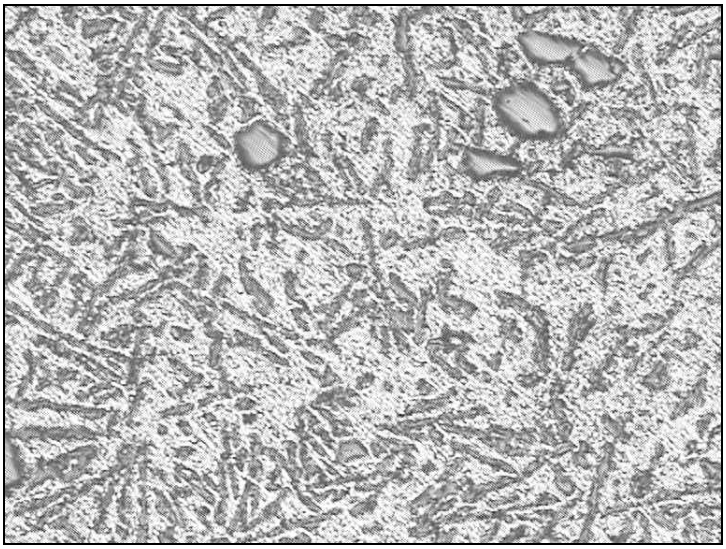

Figure 6.14: Micrograph of Sample-4, Al -12.6%Si -4.5%Cu -4.5%Cd at 200X.

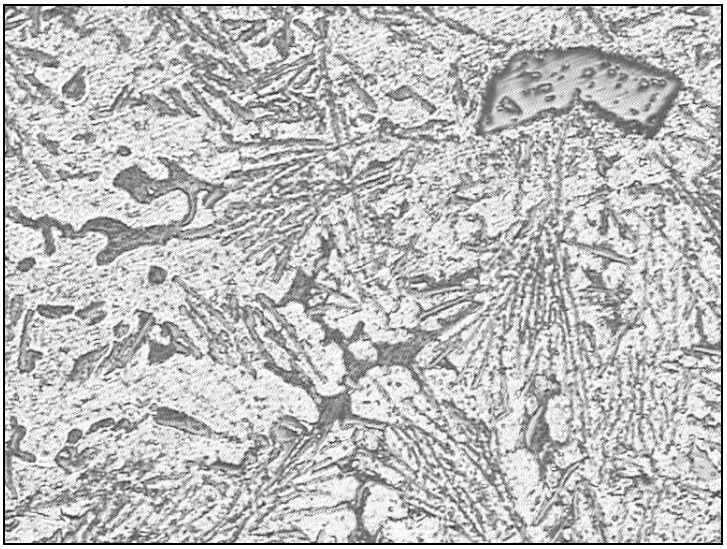

Figure 6.15: Micrograph of Sample-5, Al -12.6%Si -4.5%Cu -4.5%Bi at 200X.

Similarly as in case of set-I, in the IInd set of samples the addition of copper leads to the formation of more primary phase as compares to silicon eutectic phase. A coarse plate-like Si morphology is observed (figure 6.11). The modifiers which are in the form of immiscible substances increase the volume fraction of eutectic phase.

The growth morphology observed in the case of Pb and Sn addition leads to variation in structure. On addition of Pb coarse needles of Si are observed irregularly distributed in the matrix phase as shown in micrograph figure 6.12.

The addition of Cd allows the formation of more primary phase with fine distribution of Si needles. The features apparently indicate the dissolvation of primary silicon which ultimately gets transform to Si-eutectic structure (figure 6.14).

The structural feature alloy containing Bi is quite different as compare to other alloys. The Bi segregates along the dendrites as interdendritic liquid. The feathery growth of the Si-phase which is eutectic phase is observed all along the structure (figure 6.15).

.

6.2.2 Optical micrographs of after aging treatment

6.2.2.1 Micrographs of Set-I

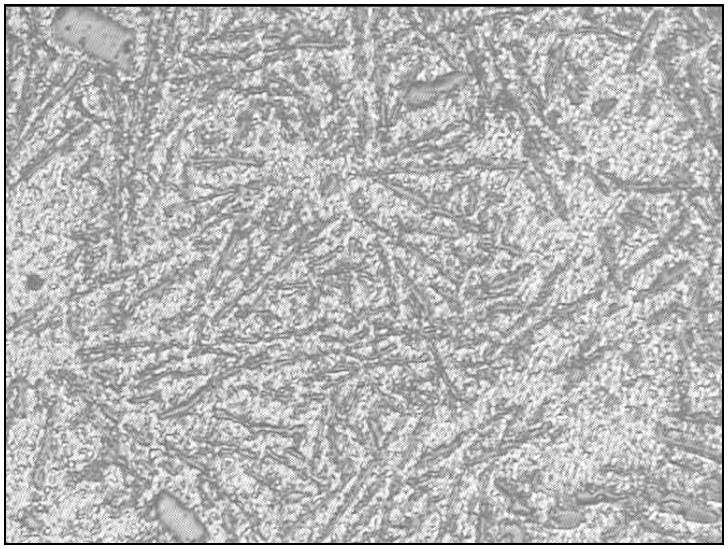

Figure 6.16: Micrograph of Sample-1 Al -12.6%Si at 400X.

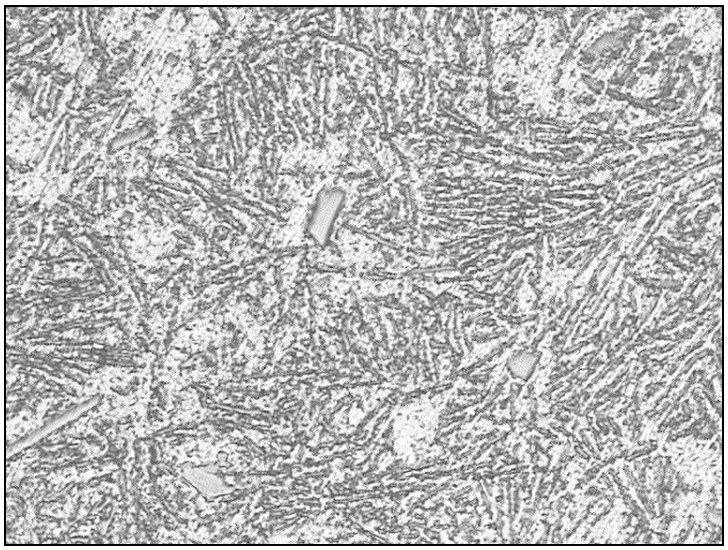

(a)

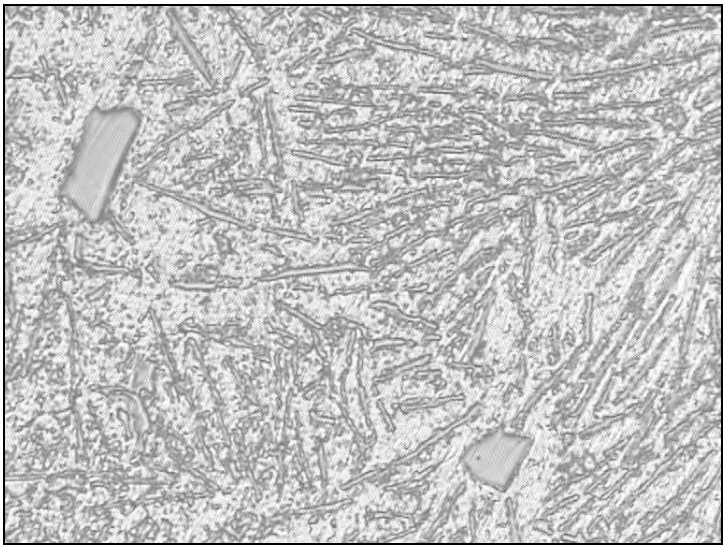

(b)

Figure 6.17: Micrograph of Sample-2 Al -12.6%Si -4.5%Pb at (a) 200X (b) 400X.

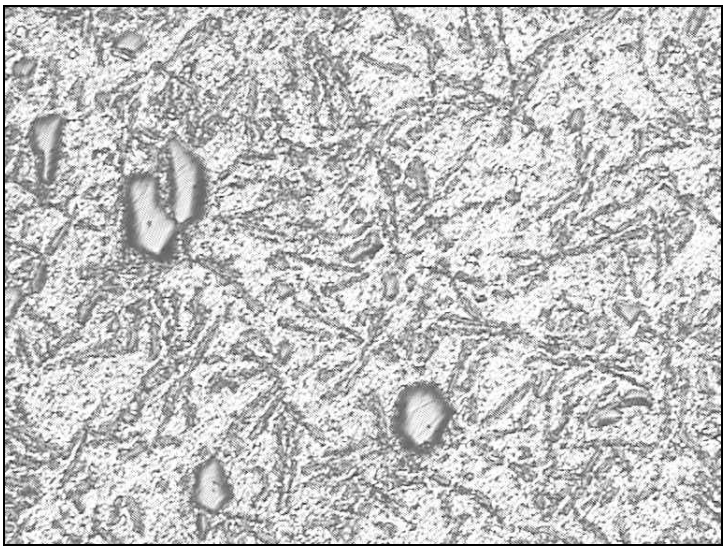

Figure 6.18: Micrograph of Sample-3 Al -12.6%Si -4.5%Sn at 200X.

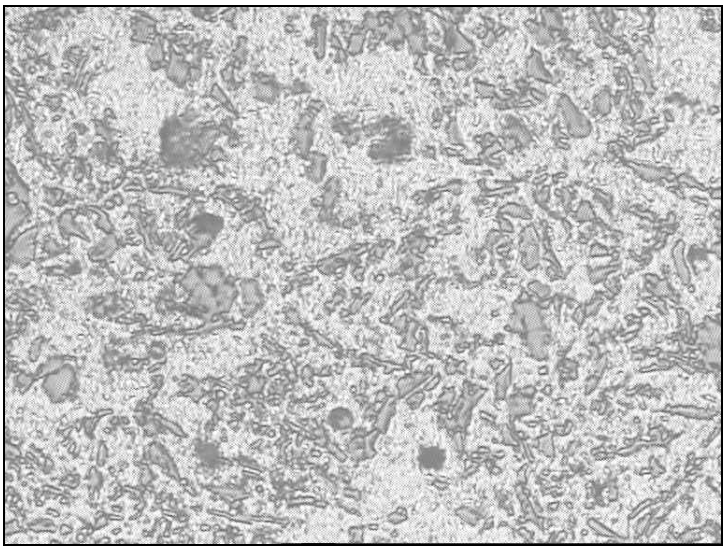

Figure 6.19: Micrograph of Sample-4 Al -12.6%Si -4.5%Cd at 400X.

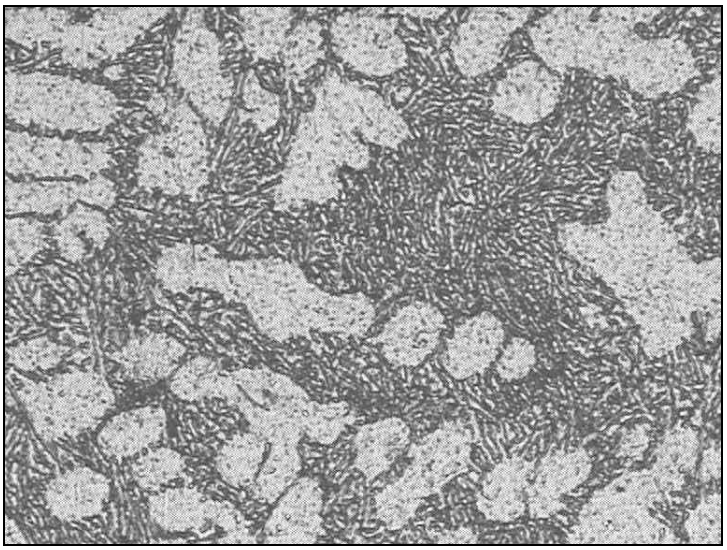

Figure 6.20: Micrograph of Sample-5 Al -12.6%Si -4.5%Bi at 200X.

6.2.2.2 Micrographs of Set-II

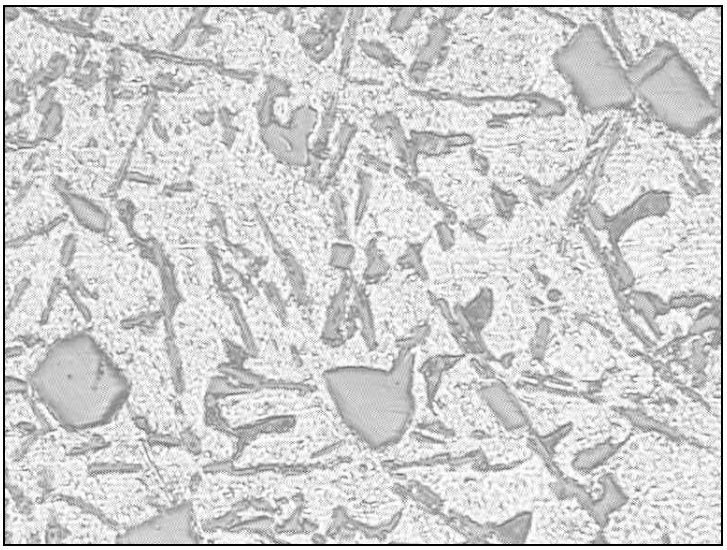

Figure 6.21: Micrograph of Sample-1 Al -12.6%Si -4.5%Cu at 400X.

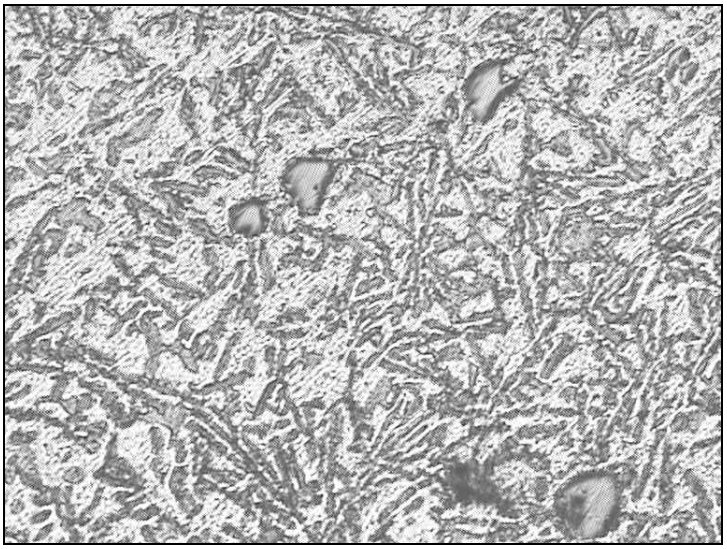

Figure 6.22: Micrograph of Sample-2 Al -12.6%Si -4.5%Cu -4.5%Pb at 200X.

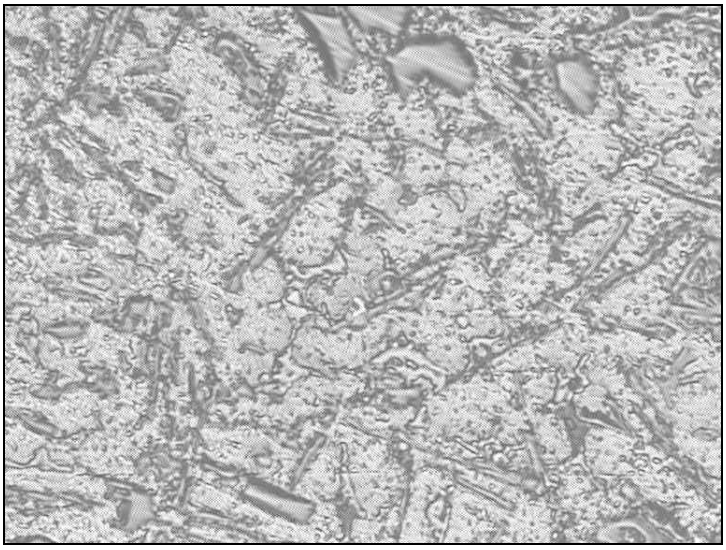

Figure 6.23: Micrograph of Sample-3,Al -12.6%Si -4.5%Cu -4.5%Sn at 400X.

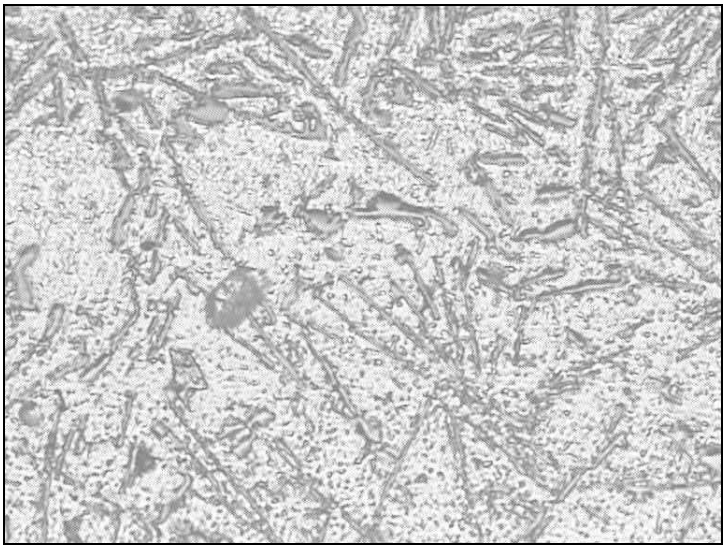

Figure 6.24: Micrograph of Sample-4 Al -12.6%Si -4.5%Cu -4.5%Cd at 400X.

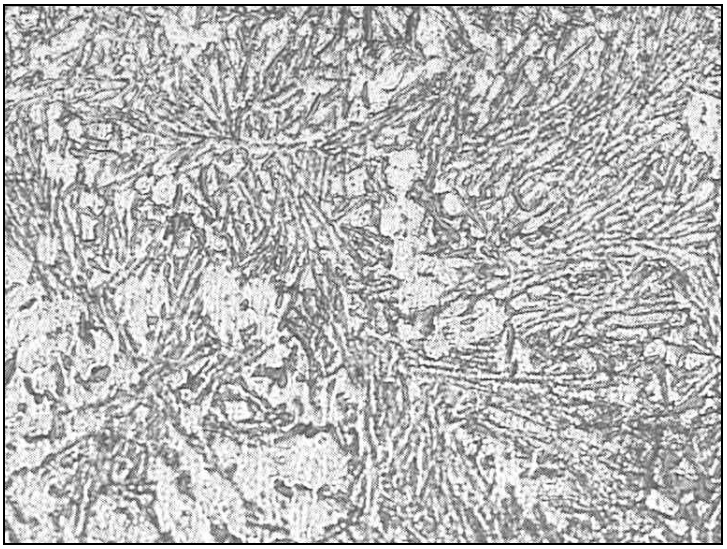

Figure 6.25: Micrograph of Sample-5 Al -12.6%Si -4.5%Cu -4.5%Bi at 200X.

Analyzing the above micrographs it was found that there is not much difference in the structural features of the alloys containing Pb, Sn and Cd (as modifiers) before and after aging process. Only some precipitate has been formed due to age hardening of the alloys. But in the case of figure 6.20 on the addition of 4.5%Bi in Al-12.6%Si alloy, a lot of variation in structural features has been observed. The grains of α-Al can be clearly visible in the fine eutectic Al-Si structure. The depression in the eutectic has been observed due to addition of Bi such that morphology changes from hyper to hypoeutectic side. This can be explained by similar results from literature as observed by W.Y. Yoon[28] on case of addition of 3% Y and 2% of Sm in Al-14%Si alloy, which had large negative mixing enthalpy with Si due to which eutectic Si crystals were modified.

6.3 Conclusions

The Al-Si near eutectic alloys containing Pb, Sn, Cd and Bi as additive element were studied. The samples of the alloys were made by the casting process consisting of the various steps such as melting, pouring and solidification of alloy in mould. After that samples are prepared for further characterization. Under characterization study microhardness and micrographical features are studied. The main aim of this work was to

prepare such bearing materials which can able to provide better toughness and compatability and good wear properties.

From the above study it can be concluded that:

1. Hardness of Al-Si increases with addition Cu. Further increase in the hardness can be obtained by heat treating the Al-Si-Cu alloys.
2. Casting method can be used to develop different bearing materials (like Al-Si-Cu) at commercial level taking care of its parameters.
3. However, the hardness properties provided by Pb and Sn in Al-Si-Cu are same, but as lead being cheaper than tin can be used commercially. Since Pb, Sn, Cd and Bi being soft can be used to provide lubricant property.
4. From the micrographic study, structural features clears that the distribution of the alloying elements (Pb, Sn, Cd and Bi) are fine in the aluminium-silicon eutectic alloys.
5. The micrographic study indicates that the elements used as modifiers Pb, Sn and Cu less modifies the Si morphology in near eutectic alloys. However, on addition of Bi the morphology completely changes from hypereutectic to hypoeutectic.

REFERENCES

1. K.H. Zum Gahr**,** *Wear by hard particles*, Volume 31, Issue 10, p. 587-596 (October 1998).

2. P. D. Merica, *The Age-Hardening of Metals*, Trans. Am. Inst. Min. Metall. Eng. 99, p.13-54 (1932).

3. H.J.Rack, *Dispersion Strengthened Aluminium Alloys*, Ed. by Y.W.Kim and W.M.Grilfith, p. 649, The Minerals, Metals and Materials Society (1988).

4. S.J.Harris, H.W. Cai and P.C.Weatherbern, *Advanced composites'93*, International Conference on Advances in Composite Materials, Ed. by T.Chandra and A.K. Dhingra, The Minerals, Metals and Materials Society (1993).

5. S.Suresh, T.Christman and S.Sugimura, Scri. Mctall. 23, 1599 (1989).

6. L.Dutta, S.M.Allen and J.L.Hafley, Metall.Trans. 22A, 2553 (1991).

7. T.R.Mcnelley and P.N.Kalu, Scri. Metall. 25, 1041 (1991).

8. D.Srinivasan and M.K.Surappa, Scri. Metall. 27, 1139 (1992).

9. G.E. Dieter, Mechanical Metallurgy, (1986), McGraw Hill Inc, U.S.A.

10. Amit M Joshi, Aluminium Foundry Practice.

11. Kurz, W. and D.J. Fisher, *Fundamentals of Solidification*, Trans Tech Publications (1998).

12. Major J.F., *A Study of ultra-low growth rates of the effects of chemical additons on the solid/liquid interface of the Al/Si interface*, University of Toronto (1989).

13. A. Knuutinen, K. Nogita, S.D. McDonald and A.K. Dahle, *Modification of Al–Si alloys with Ba, Ca, Y and Yb*, Journal of Light Metals 1, p. 229–240 (2001).

14. Chang J., Moon I. and Choi C, *Refinement of Cast Microstructure of Hypereutectic Al-Si Alloys Through the Addition of Rare Earth Metals*, Journal of Materials Science, Volume 33, Number 20, pp. 5015-5023(9), (15 October 1998).

15. Sharma Rajesh, Kumar Anesh and Dwivedi D. K., *Influence of solution temperature on microstructure and mechanical properties of two cast Al-Si alloys*, Volume 21, Number 3-4, p.309-314 (2006).

16. LIRong-de, LIRun-xia, YULi and HUZhuang-qi, *Effect of Cd and Sn Addition on the Microstructure and Mechanical Properties of Al-Si-Cu-Mg Cast Alloy*, Transactions of Materials and Heat Treatment, p.113-116.

17. M.F. Moreira and R. Fuoco, *The study of characteristics of Fatigue Fractures in Al-Si Cast Components*, AFS Transactions 2006.

18. ASM Metals Handbook, *Fractography*, 9th edition, Volume 12, p.14 (1987).

19. Wang, Q. G., Apelian, D. and Lados, D. A., *Fatigue Behavior of A356-T6 Aluminum Cast Alloys. Part I. Effect of Casting Defects and Part II. Effect of Microstructural Constituents*, J. of Light Metals, Volume 1, p.73-97 (2001).

20. Stanzl-Tschegg, S. E., Mayer, H. R., Beste, A. and Kroll, S., *Fatigue and Fatigue Crack Propagation in ALSI7mg Cast Alloys under In Service Loading Conditions*, Int. J. of Fatigue, Volume 14, p.149 – 155 (1995).

21. S.P. Nikanorov, M.P. Volkov, V.N. Gurin, Yu.A. Burenkov, L.I. Derkachenko, B.K. Kardashev, L.L. Regel, W.R. Wilcox, *Structural and mechanical properties of Al–Si alloys obtained by fast cooling of a levitated melt*, Materials Science and Engineering A390, p. 63–69 (2005).

22. O.P. Bobrov, S.N. Laptev, V.A. Khonik, Fizika Tverdogo Tela 46 (2004) 457–461 (Solid State Phys. 46 (2004)).

23. J. Mahmoud, H. Frederiksson, J. Mater. Sci. 35, p.4947– 4987(2000).

24. Hengcheng Liao , Yu Sun, Guoxiong Sun, *Correlation between mechanical properties and amount of dendritic α-Al phase in as-cast near-eutectic Al–11.6% Si alloys modified with strontium*, Materials Science and Engineering A335, p.62–66 (2002).

25. Feng Wang, Huimin Liu, Yajun Ma, Yuansheng Jin, *Effect of Si content on the dry sliding wear properties of spray-deposited Al–Si alloy*, Materials and Design 25, p.163–166 (2004).

26. Dheerendra Kumar Dwivedi, *Wear behaviour of cast hypereutectic aluminium silicon alloys*, Materials and Design 27, p.610–616 (2006).

27. L. Lasa, J.M. Rodriguez-Ibabe, Effect of composition and processing route on the wear behaviour of Al–Si alloys, Scripta Materialia 46, p.477–481 (2002).

28. H.S. Kang, W.Y. Yoon, K.H. Kim, M.H. Kim, Y.P. Yoon, I.S. Cho, *Effective parameter for the selection of modifying agent for Al–Si alloy*, Materials Science and Engineering A 449–451, p.334–337 (2007).